THE PENNSYLVANIA STATE UNIVERSITY
SCHREYER HONORS COLLEGE

DEPARTMENT OF BIOENGINEERING

THE EFFECTS OF HEMATOCRIT AND ROTATION TIME
ON PLATELET ADHESION TO A POLYURETHANE UREA SURFACE

LAUREN ELIZABETH GRUNENWALD
SPRING 2013

A thesis
submitted in partial fulfillment
of the requirements
for a baccalaureate degree
in Bioengineering
with honors in Bioengineering

Reviewed and approved by the following:

Keefe B. Manning
Associate Professor of Bioengineering and Surgery
Thesis Supervisor and Honors Advisor

Margaret J. Slattery
Assistant Professor of Bioengineering
Faculty Reader

Christopher A. Siedlecki
Professor of Surgery and Bioengineering
Faculty Reader

*Signatures are on file in the Schreyer Honors College.

ABSTRACT

Cardiovascular disease (CVD) has been the leading cause of death in the United States since 1900. CVD affects nearly 82.6 million American adults, and, on average, it claims one life every 39 seconds. Ventricular assist devices are a viable option for sustaining patients awaiting cardiac transplantation, but postoperative complications, such as bleeding, infection, and thrombosis, still remain an issue. Platelet adhesion to the plasma protein-coated polyurethane urea (PUU) blood sac in the Penn State 50 cc ventricular assist device is a primary event in thrombosis. Prior to adhesion, platelets must be convected to the material surface. Red blood cells have been shown to increase platelet diffusivity as a function of shear rate through localized mixing and cell-cell collisions and as a function of shear rate and hematocrit through platelet margination. In this study, we aim to determine the effects of hematocrit (Hct) and rotation time on platelet adhesion to PUU. A rotating disk system is used to provide a steady waveform to the PUU surface. The disk is rotated in either 20% Hct or 40% Hct reconstituted whole bovine blood for 0.5, 1, or 2 hours. Adhered platelets are immunofluorescently labeled with a primary CAPP2A mouse anti-bovine antibody and a secondary Alexa-Fluor 488 donkey anti-mouse IgG, and the PUU material is imaged at specific locations using confocal microscopy. The shear rate at each imaging location is experimentally determined using laser Doppler velocimetry. Platelet adhesion is quantified by the average platelet counts at each radial location and by calculating an adhesion coefficient from the average platelet count, platelet flux, and rotation time. The platelet fluxes and raw counts are lowest at the disk centers and increase logarithmically with shear rate. The platelet counts are an order of magnitude greater in whole blood than platelet rich plasma. After two hours of rotation, the adhesion coefficients were highest at the disk

centers and were approximately 0.15% for the 20% Hct condition and 0.20% for the 40% Hct condition.

TABLE OF CONTENTS

LIST OF FIGURES

Section 4.4

Appendix

LIST OF TABLES

LIST OF SYMBOLS

τ_s	Shear stress
η	Dynamic viscosity
x	Distance from disk center
ω	Angular velocity
υ	Kinematic viscosity
r	Radius or radial direction
u	Velocity component in the r-direction
v	Velocity component in the θ-direction
w	Velocity component in the z-direction
ρ	Density
p	Pressure
t	Time
ζ	Similarity variable
AC	Adhesion coefficient
N	Average number of platelets per unit area
j	Platelet flux
D_{eff}	Effective diffusivity
C_∞	Bulk platelet concentration
D_{SF}	Stationary flow diffusivity
D_p	Particle diffusivity

D_f	Brownian diffusivity
ϕ	Hematocrit
K_B	Boltzmann constant
T	Absolute temperature
b	Average platelet radius
k	Experimental constant
n	Experimental constant
a	Average red blood cell radius
γ	Shear rate

ACKNOWLEDGEMENTS

There are many people to whom I owe my sincerest gratitude. I would first like to thank Dr. Keefe Manning for serving as both my thesis advisor and my friend. His humor, encouragement, insight, and guidance were much appreciated and absolutely essential in completing this work. I would also like to thank Dr. Steven Deutsch for sharing his vast knowledge of all things artificial heart and fluid dynamics related. His editing expertise was much needed and his sarcastic wit much enjoyed. Thank you to Dr. Maggie Slattery and Dr. Chris Siedlecki for serving on my thesis committee and providing me with feedback on my project. I would also like to thank all former and current Artificial Heart Lab members. This is truly a one of a kind group, and I have enjoyed all of the laughs both inside and outside of Hallowell. A special thanks to Josh Taylor, Ben Knisely, and Alex Smith for taking all of the LDV data.   Thank you to Dr. Lichong Xu who prepared all of the PUU samples and to Nadine Houck and Travis Edwards who drew blood for me on many mornings.

I would also like to thank my friends and family who have supported me during my five years at Penn State. Thank you for your kind words, constant encouragement, and willingness to listen to my countless rants. I would like to thank Mike Navitsky who patiently taught me the RDS protocol while simultaneously doubling as my boyfriend. Thank you for your positive perspective, voice of reason, and willingness to put up with my endless sass. Lastly, and most importantly, I would like to thank my parents, Bill and Ginny Grunenwald, for their unwavering love and support. Thank you for providing me with so much and for reminding me that I am capable of more than I often think I am. I love you.

Chapter 1

Introduction

1.1 Clinical Need

Cardiovascular disease (CVD), which includes patients suffering from angina, hypertension, heart failure, myocardial infarction, and stroke, affects an estimated 82,600,000 (>1 in 3) American adults and has been the leading cause of death in the United States every year since 1900 (except 1918). On average, CVD claims one American life every 39 seconds, and deaths attributed to CVD outnumber those due to cancer, chronic lower respiratory disease, and accidents combined.(1) Although certain forms of CVD can be treated by lifestyle change, medication, catheterization, and invasive surgical procedures, such as valve replacements, total heart transplantation is sometimes required.

After a transient spike in the number of heart transplantations during the mid-1990s, the number of cardiac transplant procedures performed per year in the United States has leveled off to around 3,700.(2) On any given day, the National Heart, Lung, and Blood Institute estimates that approximately 3,000 patients are on the heart transplant waiting list.(3) The amount of time a patient spends on the waiting list depends on many factors, including age, blood type, and condition. Although this time can vary from days to years, in 2004, the Organ Procurement and Transplantation Network reported that the median wait time for patients between the ages of 18 and 64 was approximately 169 days.(4) In response to limited donor availability and extensive wait times, researchers and physicians have turned to mechanical circulatory support devices as a means for sustaining patients awaiting cardiac transplantation.

1.2 Ventricular Assist Devices

Ventricular assist devices (VADs) have been a viable option for adult patients requiring bridge-to-transplant mechanical circulatory support since the HeartMate LVAS received FDA approval in 1994.(5) VADs are surgically implanted blood pumps that work in parallel with a patient's native ventricle to supply blood to the body. Although VADs can be placed in a left, right, or bi ventricular configuration, left ventricular assist devices (LVADs) are most common due to the relatively high systemic resistance against which the left ventricle must pump. Thus, the majority of VADs pump blood from the left ventricle to the aorta.

In 2001, the Randomized Evaluation of Mechanical Assistance for the Treatment of Congestive Heart Failure (REMATCH) study sought to determine the sustainability of long-term LVAD use by comparing HeartMate XVE LVAD patient outcomes to the outcomes of patients receiving advanced medical therapy alone. The results demonstrated that LVAD implantation more than doubled the 1-year survival rate (52%) compared to patients solely receiving optimal medical management (25%). Additionally, the LVAD patients experienced an increased quality of life, both physically and emotionally. However, the morbidity and mortality associated with LVAD implantation were still concerning.(6) Therefore, in 2007, a post-REMATCH era study was conducted to further investigate LVAD performance for end-stage heart failure patients using a modified version of the HeartMate XVE LVAD. With these modifications came improved safety and reliability, an improved general understanding of mechanical circulatory support, and a slight increase in the 1-year survival rate (56%). However, the incidence of postoperative complications remained high.(7) Since this study, LVADs have been improved through an iterative design process,

and in 2011, the 1-year survival rate for clinically used devices neared 85%, a result comparable to intermediate-term heart transplantation outcomes.(8)   Postoperative complications, such as bleeding, infection, and thrombosis, however, still remain an issue.

1.3 Penn State 50 cc Ventricular Assist Device

Penn State's Artificial Heart Program began as a collaborative effort between the College of Medicine and the College of Engineering in 1970. The first assist device consisted of a flexible segmented polyurethane sac housed in a polycarbonate case, inlet and outlet cannulas fitted with ball and cage valves, a pneumatic driver, a synchronizer, and a monitoring apparatus. This initial pulsatile VAD was intended for patients who were unable to be weaned from cardiopulmonary bypass after surgery.(9) In 1976, an iteration of this original design, shown in Figure 1.3.1, received FDA approval for investigational applications. Soon after, Thoratec Corporation began manufacturing the paracorporeally-placed Pierce-Donachy VAD for nationwide use.(10)
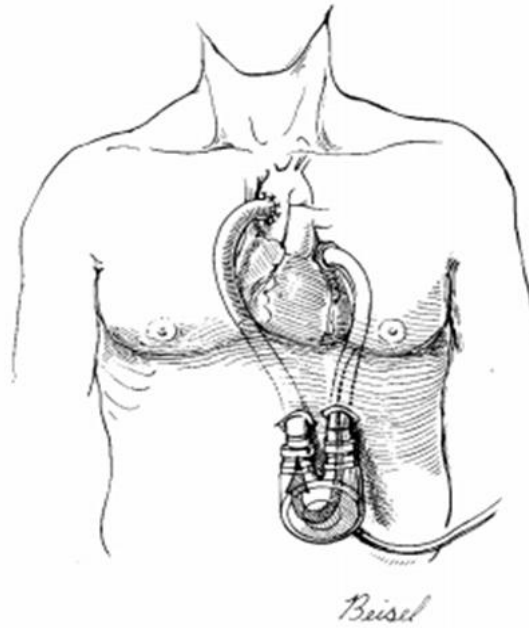
Figure 1.3.1 An artist's rendition of the Pierce-Donachy VAD, illustrating the pump's paracorporeal placement.(10)

After realizing that a similar device could be used to sustain patients awaiting cardiac transplantation, the group's focus shifted toward developing an implantable VAD. With the advent of a transcutaneous energy transmission system, an electronically-driven VAD that allowed for increased patient mobility was developed in two sizes: an experimental model with a 100 cc stroke volume and a clinical model with a 70 cc stroke volume.(11) The 70 cc model underwent successful *in vitro* and *in vivo* testing and was implanted in more than 250 patients worldwide with a success rate of over 90%.(12) By 2001, Penn State had partnered with Arrow International to bring this device, commercially known as the Arrow LionHeart LVD 2000, to clinical trials.(13) The design, however, was limited by patient chest cavity size. Consequently, the 70 cc device was scaled down to 50 cc in order to accommodate average size women and men of small stature.(14) Initial *in vitro* particle image velocimetry

(PIV) studies and *in vivo* animal studies showed a correlation between regions of flow stasis and low wall shear rates and thrombus deposition in the 50 cc device.(15, 16) It was hypothesized that the smaller device's lower Reynolds numbers resulted in decreased mixing, increased fibrin and platelet deposition, and, therefore, increased thrombus susceptibility. Since these initial experiments, the 50 cc device has been studied extensively and further modified. PIV studies have been used to determine how global flow characteristics are affected by altered beat rates and systolic durations and by modifications to the mitral valve and outlet port orientations.(17–19) Most recently, a thrombus susceptibility metric was used to compare two 50 cc design iterations.(20)

1.4 Polyurethane Urea Biocompatibility

Biocompatibility is defined as "the ability of a material to perform with an appropriate host response in a specific application."(21) Given the integral dependence of a material's performance on the particular application, it is inappropriate to describe a material as being uniformly biocompatible. The concept of biocompatibility must be considered in medical device design, as the reaction of the native tissue to the foreign material will dictate how well the device performs physiologically.(22)

Polyurethanes have been widely used in medical devices since the 1950s, largely due to their desirable biomaterial characteristics. Polyurethanes possess excellent abrasion and chemical resistance as well as tensile and tear strength, and due to their segmented structure, they have unique and variable combinations of toughness, flexibility, and durability. Their variable chemical and physical makeups lend them to a variety of medical device applications, including medical tubing, drug delivery devices, IV connectors, and transdermal

patches. Additionally, polyurethanes exhibit good hemocompatibility, making them a common material choice in cardiovascular devices, such as catheters, pacemakers, intra-aortic balloons, and VADs.(23)

Given that thromboembolism is the most frequent and serious complication associated with mechanical circulatory support devices, hemocompatibility is one of the main concerns when designing and evaluating ventricular assist devices. VADs are especially susceptible to thrombus formation because of their long-term use, large surface areas, and complex flows.(24) In 1856, Rudolph Virchow postulated that the three factors affecting thrombosis, collectively referred to as Virchow's Triad, are the blood flow, the blood-contacting surface, and the blood constituents.(25) The blood flow within the 50 cc device has been extensively studied.(16–20) The blood-contacting material (the second factor in Virchow's Triad) used in the Penn State 50 cc VAD is polyurethane urea (PUU), a polyurethane derivative, commercially known as BioSpan MS/0.4 (The Polymer Technology Group, Berkeley, California). This material consists of a methylenediisocyanate hard segment, a polytetramethylene oxide soft segment, and an ethylene diamine chain extender. The polymer is endcapped with 2000 molecular weight polydimethylsiloxane (PDMS) at 0.4% by weight.(26)

Blood is a complex connective tissue that contains gases, ions, nutrients, hormones, proteins, chemical wastes, lipids, platelets, and various nucleated cells.(27) These components constitute the third factor of Virchow's Triad, but platelets and plasma proteins play the most significant roles in thrombosis. Platelets are anuclear discoid bodies that result from the fragmentation of megakaryocyte cytoplasm.(28, 29) Platelets are found at physiologic plasma concentrations of 150×10^6-350×10^6 platelets/mL.(30) In the absence of a

stimulus, platelets remain in a quiescent state and do not contribute to coagulation. However, in the presence of an activating stimulus, such as collagen fiber exposure, adhesion protein adsorption, or bulk phase agonists, platelets become activated and accelerate thrombosis.(29) High shear or a sudden increase in shear can also activate platelets.(31) An electron micrograph of a resting platelet and two activated platelets is shown in Figure 1.4.1. Pseudopodia formation, as depicted in Figure 1.4.1, is a classic indicator of platelet activation.
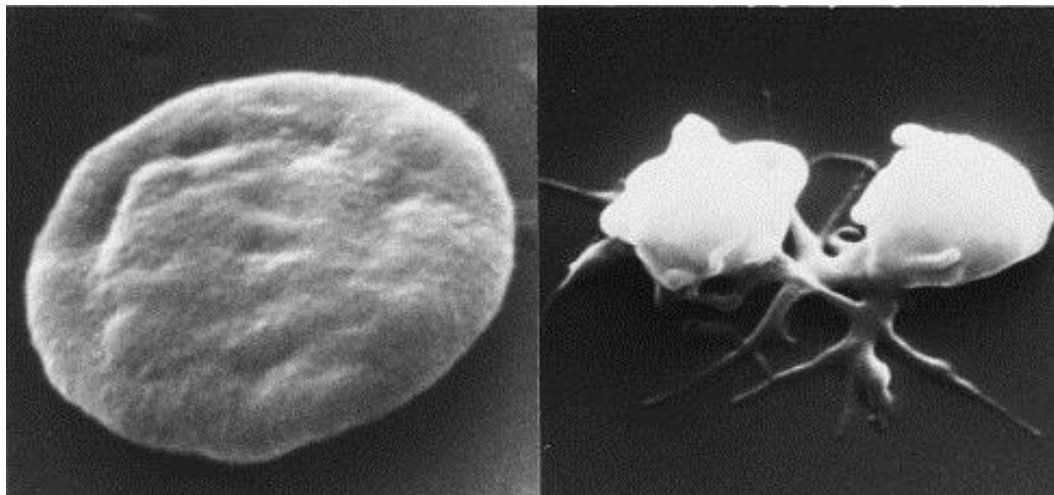
Figure 1.4.1 Electron micrograph of a resting platelet (left) and two activated platelets exhibiting pseudopodia formation (right).(28)

Of these activating mechanisms, adhesion protein adsorption is the stimulus most commonly associated with biomaterial-mediated thrombosis. As a result of interfacial energetics, plasma proteins in flowing blood adsorb to polymer surfaces within seconds after contact, stabilized by hydrogen bonding and van der Waals, hydrophobic, and electrostatic

interactions.(32, 33)   It has been shown that the amount of adsorbed protein and the conformation of the adsorbed proteins affect platelet adhesion.(34)   One study compared plasma protein adsorption and platelet adhesion to poly(2-methoxyethylacrylate) (PMEA) and poly(2-hydroxyethylmethacrylate) (PHMEA) surfaces. Plasma protein adsorption was low for both surfaces. However, the proteins adsorbed to the PMEA surface showed little conformational change from their native states, while the conformation of the proteins adsorbed to the PHMEA surface changed considerably. Platelet adhesion was significantly less on the PMEA surface, suggesting that platelet adhesion is reduced when plasma proteins maintain their native conformations after adsorption.(34)   In addition to biomaterial selection, many groups now focus on modifying surface chemistries and topographies to decrease protein adsorption and platelet adhesion.(33)

The principle adhesion proteins involved in biomaterial-mediated thrombosis are fibrinogen, fibronectin, vitronectin, and von Willebrand factor (vWF). The physiologic plasma concentrations of these proteins are 3.0 mg/mL, 0.3 mg/mL, 0.3 mg/mL, and 0.05 mg/mL, respectively. These adhesion proteins stimulate platelets through interactions with the GPIIb-IIIa, GPIb-IX, $\alpha_v\beta_3$, and $\alpha_5\beta_1$ platelet surface receptors. Figure 1.4.2 shows the glycoprotein receptors, GPIIb-IIIa and GPIb-IX, interacting with fibrinogen and vWF. These interactions increase the platelets' procoagulant activity through intracellular signaling cascades, resulting in both platelet adhesion and platelet activation. Upon activation, platelets further accelerate thrombosis by secreting bulk phase agonists, such as adenosine diphosphate, secreting coagulation cascade cofactors, such as Ca^{2+}, mediating platelet-platelet aggregation, and increasing thrombin production.(29)

Figure 1.4.2 A platelet and its glycoprotein receptors. vWF binds to the GPIb-IX receptor, and fibrinogen binds to the GPIIb-IIIa receptor. vWF can also bind to the GPIIb-IIIa and $\alpha_v\beta_3$ receptors.(35)

Therefore, when designing ventricular assist devices, platelet adhesion and activation should be minimized in order to reduce thrombosis. Although the individual factors of Virchow's Triad are relatively well understood when studied independently, thrombus formation is an intricate and complex process. This complexity is derived from the inherent interconnectedness of the three factors. Therefore, we must consider not only the three factors but also how these factors relate to and affect one another.

1.5 Previous Studies

Hubbell and McIntire used epifluorescent video microscopy to visualize the cell-cell and cell-surface interactions of thrombosis in real-time for collagen, polyurethane, and nylon surfaces. Whole blood was passed through a parallel-plate flow chamber at several constant shear rates for each material, and digital image processing was used to analyze the morphological features and the number of platelets of individual thrombi. At 100 s^{-1}, many small to moderate thrombi (<20 platelets) formed on polyurethane but were quickly embolized. Although the number of deposited platelets was small, the rate of embolism from the surface was high (0.25/(100 μm^2·min)). At 500 s^{-1}, however, many temporary (<1 second) individual platelet adhesions were observed. These individual platelets attached at a rate of approximately 2.5/(100 μm^2·min), yet few large emboli formed and no stable thrombi remained on the surface. These findings suggest that platelets are unable to form stable surface bonds to plasma proteins on polyurethane at shear rates greater than 500 s^{-1}.(36)

Rotating disk studies have been used to investigate cellular adhesion to biomaterials. A rotating disk is desirable, as the flow field near the disk surface has been extensively studied and is well understood.(37–39) By using the linear relationship between shear rate and radial distance, we can investigate over a wide shear range that we can easily manipulate. One rotating disk study analyzed the effects of adsorbed platelet and plasma proteins on the adhesion of *Staphylococcus epidermidis* to polyethylene, another biomaterial commonly used in cardiovascular devices.(40) A physiologic shear stress range of 0-73 dyne/cm^2 was investigated, and an adhesion coefficient was used to quantitatively evaluate bacterial adhesion. It was shown that while adsorbed plasma proteins decrease bacterial adhesion relative to a bare polyethylene surface, adsorbed platelets increase bacterial adhesion by an

order of magnitude. These results suggest that platelet adhesion mediates bacterial adhesion, device infection, and sepsis.(40)

A second rotating disk study investigated the effects of sub-micron PUU texturing on platelet adhesion.(26) Two sub-micron pillar schemes were fabricated on PUU samples, and a rotating disk was used to generate a physiologic shear stress range of 0-67 dyne/cm^2. Although platelet adhesion was found to be greatest from 0-5 dyne/cm^2, sub-micron texturing was found to reduce platelet adhesion in this range. Additionally, from 0-9.5 dyne/cm^2, platelet adhesion decreased with increasing shear stress, with the greatest adhesion seen at 0 dyne/cm^2. At higher shear stresses, however, the adhesion coefficient was lower yet remained constant with shear stress, and there was no significant difference in platelet adhesion between the textured and untextured PUU samples. These results suggest that sub-micron texturing may help to reduce platelet adhesion in areas of low shear stress by reducing the surface area available for platelet interactions.(26)

Most recently, the rotating disk was used to examine how peak shear exposure affects platelet adhesion.(41) Five waveforms, each with a root mean square (RMS) angular velocity of 29.63 rad/s and a period of 700 ms, were investigated. A steady waveform served as a baseline. A cardiac pulse waveform, with a peak angular velocity of 54.35 rad/s, was extracted from the 50 cc Penn State VAD inlet flow probe. Three ramp waveforms were also investigated. The first ramp waveform reached a peak angular velocity that was 25% greater than the cardiac pulse peak value. The second ramp waveform had a peak angular velocity equal to that of the cardiac waveform, and the third ramp waveform had a peak angular velocity that was 25% less than the peak cardiac pulse value. Platelet adhesion was found to decay exponentially with increasing shear rate. For shear rates less than 500 s^{-1}, peak shear

exposure directly influences platelet adhesion. At higher shear rates, however, platelet adhesion depends solely on RMS shear levels. At shear rates greater than 1000 s^{-1}, platelet adhesion is rare.(41)

1.6 Current Study

Previous rotating disk platelet adhesion studies have been conducted using platelet rich plasma, rather than whole blood, as the fluid medium. This approach is beneficial, as platelet rich plasma is a Newtonian fluid, and the shear stresses in the rotating disk boundary layer can be directly calculated using the following equation:

$$\tau_s = 0.8\eta x (\frac{\omega^3}{\upsilon})^{1/2} \tag{1}$$

where η is the dynamic viscosity, x is the radial distance from the disk center, ω is the angular velocity, and υ is the kinematic viscosity. The corresponding shear rates can be calculated by simply dividing the shear stress by the dynamic viscosity. Using whole blood complicates this calculation, as blood is a shear-thinning fluid. Therefore, these calculations do not hold.

Using whole blood, however, is an important next step, as platelet diffusivity in whole blood is several orders of magnitude greater than platelet diffusivity in plasma alone.(42) This increase is due to the presence of red blood cells (RBCs).(43) Specifically, localized RBC mixing increases platelet diffusivity, and in vessel flow, RBCs concentrate at the vessel center, effectively increasing the platelet concentration near the walls.(43, 44)

There are two basic types of RBC mixing: the rotation of individual cells and mixing due to cell-cell collisions. Both types, however, are due to shearing effects.(43) When an RBC is acted upon by varying shear, the RBC rotates, and frictional forces cause the fluid surrounding the cell to rotate as well. This type of mixing augments the transport of the platelets found within these rotating fluid elements.(43) The cell-cell interactions are similar to the intermolecular collisions of Brownian motion but on a macroscopic scale. As platelet-containing fluid elements flow into the spaces vacated by RBCs post-collision, platelet diffusivity increases.(45) Platelet marginalization is a function of both hematocrit and shear.(44) In tube flow, RBCs are concentrated at the center of the vessel, and platelets are forced to the near wall region. This increases the near wall platelet concentration and in turn increases platelet adherence.(44)

These phenomena have been studied both experimentally and computationally. In one study, suspensions of washed human platelets and reconstituted blood samples were flowed through an axi-symmetric glass expansion tube coated with collagen fibers.(46) This study demonstrated that high hematocrit and platelet concentrations and regions of high wall shear stress correlated with elevated platelet deposition.(46) This experimental setup was also modeled computationally, and similar results were observed.(47)

Here, we seek to understand the effects of hematocrit (Hct) and rotation time on platelet adhesion to the PUU material using a rotating disk. Both 20% and 40% reconstituted whole blood samples are investigated for rotation periods of 0.5, 1.0, and 2.0 hours. Platelet adhesion is quantified, and the relationships between hematocrit, rotation time, shear rate, and platelet adhesion are investigated.

Chapter 2

Theory

2.1 Rotating Disk Flow

Flow due to a rotating disk was originally solved by von Karman using a momentum-integral solution in 1921 and was later improved upon by Cochran's numerical solution in 1934.(37, 38) The following explanation is based on Benton's 1966 steady state and time-dependent, initial-value solutions.(39)   The continuity (Equation 2) and Navier-Stokes (Equations 3-5) equations for non-steady, axially-symmetric, incompressible flow of a homogenous fluid are as follows:

$$(ru)_r + (rw)_z = 0 \tag{2}$$

$$u_t + uu_r + wu_z - r^{-1}v^2 = -\rho^{-1}p_r + \nu[u_{rr} + (r^{-1}u)_r + u_{zz}] \tag{3}$$

$$v_t + uv_r + r^{-1}uv + wv_z = \nu[v_{rr} + (r^{-1}v)_r + v_{zz}] \tag{4}$$

$$w_t + uw_r + ww_z = -\rho^{-1}p_z + \nu[w_{rr} + r^{-1}w_r + w_{zz}] \tag{5}$$

where u, v, and w are velocity components in the r, θ, and z directions, respectively, ρ is the density, ν is the kinematic viscosity, and p is the pressure. Subscripts represent derivatives. For flow induced by a rotating disk that starts from rest and reaches steady rotation with a constant angular velocity, ω, the initial and boundary conditions are as follows:

$$at\ t = 0:\ u = v = w = 0 \tag{6}$$

$$at\ z = 0:\ u = w = 0, v = r\omega \tag{7}$$

$$as\ z \to \infty:\ u, v \to 0 \tag{8}$$

The streamlines for flow due to a rotating disk are shown in Figure 2.1.1. It should be noted that only the bottom of the disk contacted the fluid in our experiments. The rotation of the disk induces rotation of the fluid near the disk surface. Because there is no radial pressure gradient, as the fluid rotates, it is directed radially outward from the disk surface. In order to satisfy conservation of mass, axial flow is directed inward towards the disk surface.(48)
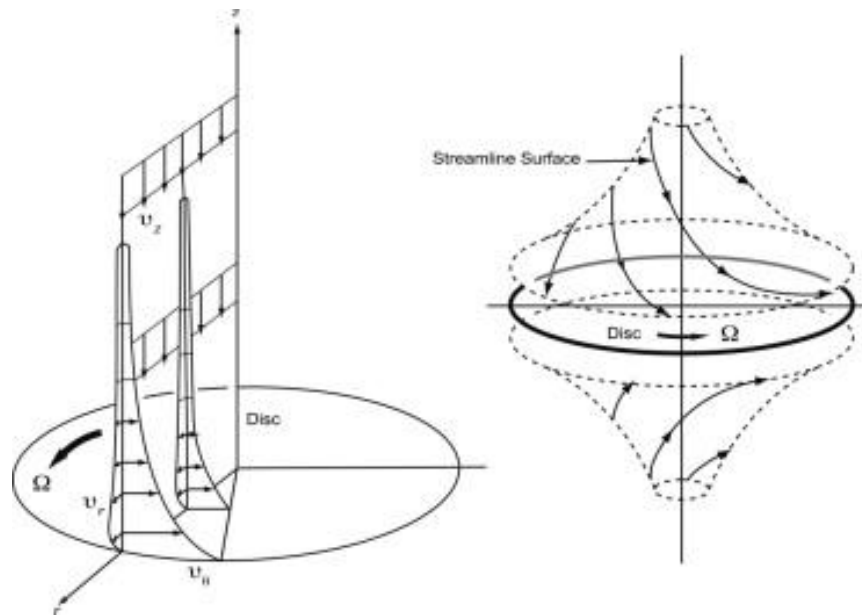
Figure 2.1.1 The streamlines in the r, θ, and z directions for flow due to a rotating disk. Fluid flows radially outward from the disk surface, and to satisfy conservation of mass, fluid is directed axially inward toward the disk surface.(48)

The similarity variable, ζ, and the similarity forms of the velocity field and pressure distribution used by von Karman are as follows:

$$\zeta = (\frac{\omega}{\nu})^{1/2}z \tag{9}$$

$$u(r,z) = r\omega F(\zeta) \tag{10}$$

$$v(r,z) = r\omega G(\zeta) \tag{11}$$

$$w(z) = (\nu\omega)^{\frac{1}{2}}H(\zeta) \tag{12}$$

$$p(z) = -\rho\nu\omega P(\zeta) \tag{13}$$

Equations 9-13 are transformed into Equations 14-17.

$$H' + 2F = 0 \tag{14}$$

$$F'' - HF' - F^2 + G^2 = 0 \tag{15}$$

$$G'' - HG' - 2FG = 0 \tag{16}$$

$$P' - HH' + H'' = 0 \tag{17}$$

The following boundary conditions result:

$$G(0) = 1 \tag{18}$$

$$F(0) = H(0) = G(\infty) = F(\infty) = 0 \tag{19}$$

16

After substituting Equation 13 into Equations 14 and 15, the following alternative boundary-value problem arises:

$$G'' - HG' + H'G = 0 \tag{20}$$

$$H''' - HH'' + \frac{1}{2}H'H' - 2G^2 = 0 \tag{21}$$

$$G(0) = 0 \tag{22}$$

$$H(0) = H'(0) = G(\infty) = H'(\infty) = 0 \tag{23}$$

As ζ approaches infinity, there is a finite flow towards the disk. Given this condition, Cochran defined a variable, c, as follows:

$$-c = H(\infty) \ (c > 0) \tag{24}$$

G and H are then expressed as the following expansions:

$$G \sim A_1 e^{-c\zeta} + A_2 e^{-2c\zeta} A_3 e^{-3c\zeta} + \cdots \tag{25}$$

$$H \sim -c + B_1 e^{-c\zeta} + B_2 e^{-2c\zeta} + B_3 e^{-3c\zeta} + \cdots \tag{26}$$

Given these expansions, the similarity variable is redefined by Equation 27, and Equations 20 and 21 are rewritten as Equations 28 and 29 with corresponding boundary conditions (Equations 30-31).

$$\lambda = e^{-c\zeta} \tag{27}$$

$$\lambda g'' + hg' - h'g = 0 \tag{28}$$

$$\lambda^3 h''' + 2\lambda^2 h'' + \lambda^2 hh'' + \lambda hh' - \frac{1}{2}\lambda^2 h'h' + 2g^2 = 0 \tag{29}$$

$$c^2 g(1) = 1 \tag{30}$$

$$g(0) = h(0) = h'(1) = 0 \tag{31}$$

$$h(1) = 1 \tag{32}$$

After rewriting g and h in terms of power series expansions, the following set of equations can be used to determine the three-dimensional velocity field and pressure distribution.

$$g(\lambda) = a_1\lambda + a_2\lambda^2 + a_3\lambda^3 + \cdots = \sum_{i=1}^{n} a_i\lambda^i \tag{33}$$

$$h(\lambda) = b_1\lambda + b_2\lambda^2 + b_3\lambda^3 + \cdots = \sum_{j=1}^{n} b_j\lambda^j \tag{34}$$

$$a_i = \frac{1}{i(i-1)} \sum_{k=1}^{i-1} [(i-2k)a_k b_{i-k}] \quad (i = 2,3,4,\dots,n) \tag{35}$$

$$b_j = -\frac{1}{2j^2(j-1)} \sum_{k=1}^{j-1} [(j-k)(2j-3k)b_k b_{j-k} + 4a_k a_{j-k}] \quad (j = 2,3,4,\dots,n) \tag{36}$$

18

Chapter 3

Methods

3.1 Polyurethane Urea Sample Preparation

All of the PUU samples were manufactured at the Hershey Medical Center (Hershey, Pennsylvania) using a successive spin casting and curing protocol.(26) The samples, which were made from 18% Biospan MS/0.4, were created in three consecutive layers using a smooth PDMS mold. The first, second, and third layers were each spun for 60 seconds at 1500 rpm, 800 rpm, and 400 rpm, respectively. After each spin casting, the sample was allowed to cure overnight in a vacuum at room temperature. This procedure maintains sample smoothness while also increasing sample thickness. A stamp was used to cut a 20 mm diameter circular piece of PUU, and this sample was mounted to a metal disk using double-sided poster tape. The mounted sample equilibrated in phosphate buffered saline (PBS) at 30°C for one hour.

3.2 Reconstituted Blood Preparation

Approximately 450 mL of whole blood was drawn from the jugular vein of a healthy female bovine at the Penn State Dairy Barn according to IACUC #31641. The blood was collected using a 16 G needle and a single collection blood bag that was pre-anti-coagulated with CPDA-1 solution (Jorgensen Laboratories, Inc., Loveland, Ohio). The blood bag was kept in an insulating container during transportation from the barn to the laboratory.

Eight 45 mL whole blood aliquots were prepared in 50 mL centrifuge tubes, and the samples were centrifuged at 600 g for 12 minutes. Acceleration and deceleration settings

were set to 1% to minimize platelet activation and mixing. After centrifugation, the top platelet rich plasma (PRP) layers were gently removed from each centrifuge tube using a 25 mL serological autopipette and transferred to clean 50 mL centrifuge tubes. The remaining blood was then centrifuged at 1500 g for 20 minutes with 1% acceleration and 1% deceleration. After this second centrifugation, the top platelet poor plasma (PPP) layers were gently removed from each centrifuge tube and transferred to clean tubes, leaving only the buffy white coat layers and RBCs behind in the original eight tubes. The buffy white layers were discarded, and the remaining RBC volumes were combined into a single tube. The centrifugation procedure is depicted in Figure 3.2.1. The separated blood components were kept in a 30°C water bath prior to reconstitution.
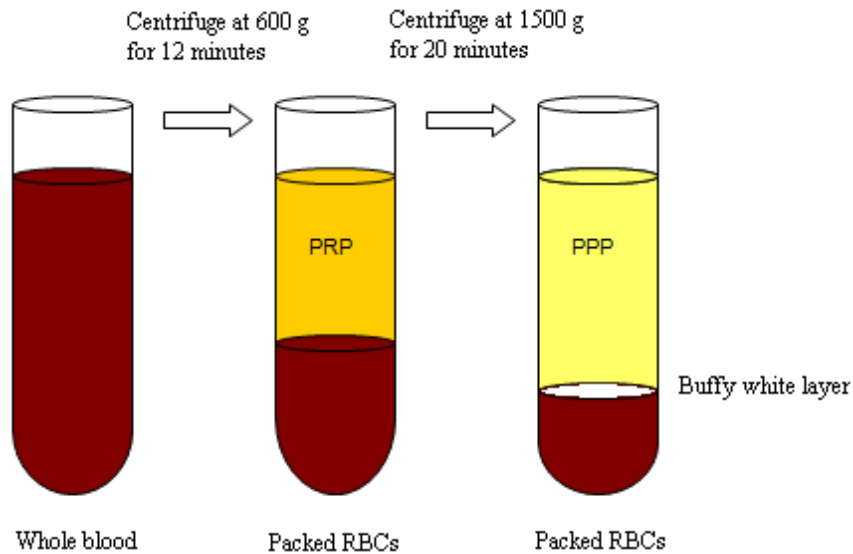
Figure 3.2.1 The centrifugation procedure. Whole blood was centrifuged at 600 g for 12 minutes. PRP was removed and saved, and the remaining blood was centrifuged at 1500 g for 20 minutes. The PPP and RBCs were removed, and the buffy white layer was discarded.

For every experiment, a 50 mL sample of reconstituted whole blood with a known hematocrit and platelet concentration was prepared. For the 40% Hct experiments, the 50 mL reconstituted blood samples contained 20 mL of packed RBCs, and for the 20% Hct experiments, the 50 mL blood samples contained 10 mL of packed RBCs. A small sample of PRP was diluted by a factor of 100 using PBS, and the initial platelet count was measured using a hemocytometer (Hausser Scientific, Horsham, Pennsylvania) and a bright field microscope (Nikon, Melville, New York) fitted with a 40x dry objective (Nikon, Melville, New York). Using the initial platelet concentration, the appropriate PRP:PPP volume ratio was determined such that the final platelet concentration for all experiments was 250×10^6 platelets/mL. The actual hematocrit values for the 20% Hct and 40% Hct reconstituted blood samples were measured using a microhematocrit centrifuge (Iris Sample Processing, Westwood, Massachusetts). All experimental Hct values were within +/- 1.5% of the theoretical values. The final 50 mL sample was gently mixed and placed into a 100 mL polytetrafluoroethylene (PTFE) beaker. The beaker was then placed on a hot plate underneath the rotating disk system to keep the temperature of the blood at 30°C for the entire experiment. The viscosity curves for both the 20% Hct and 40% Hct reconstituted blood samples were measured at 30°C using a viscometer (Vilastic Scientific, Inc., Austin, Texas).

3.3 Steady Rotation Experiments

The rotating disk system (RDS) (Pine Instrument Company, Grove City, Pennsylvania) is shown in Figure 3.3.1. The RDS motor connects to a threaded shaft, and after equilibrating in PBS for one hour, the metal disk with adhered PUU was fastened to the shaft. The metal disk is inscribed with nine concentric circles each separated by 1 mm and six radial lines each separated by 60° to determine locations during imaging. The PUU sample was lowered approximately 3 mm into the reconstituted whole blood sample and the RDS was turned on. A knob on the motor was used to manually adjust the rotation rate to 283 rpm, and the sample was rotated for 0.5 hours, one hour, or two hours.
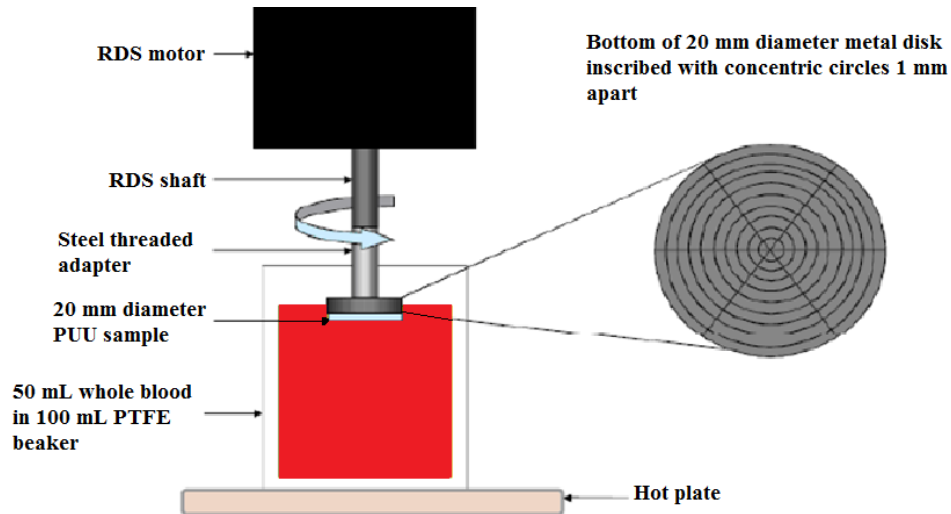
Figure 3.3.1 The rotating disk system experimental setup.(40)

After spinning for the predetermined time, the RDS motor was turned off, but the metal disk was left fastened to the shaft. An autopipette was used to gently replace the reconstituted whole blood with PBS by adding and removing six 35 mL aliquots. The PBS solution was then replaced with a 1% paraformaldehyde (PFA) solution by adding and removing six 35 mL aliquots. The PUU remained immersed in the PFA solution for one hour at 30°C to fix the adhered platelets to the PUU surface. The PFA solution was then replaced by six 35 mL aspirations of PBS, and the metal disk was removed from the RDS and placed in a 12-well polystyrene tissue culture plate.

3.4 Fluorescent Platelet Labeling and Imaging

The PUU sample was incubated in a primary CAPP2A mouse anti-bovine $\alpha_{IIb}\beta_3$ antibody (VMRD, Pullman, Washington) solution (1.50 μL CAPP2A antibody in 1 mL 6% donkey serum blocking agent (Sigma-Aldrich, St. Louis, Missouri)) and refrigerated overnight. The next day, the sample was gently washed with 5 x 3 mL PBS aspirations to remove non-specifically bound primary antibodies. The sample was then incubated in a secondary Alexa-Fluor 488 donkey anti-mouse IgG antibody (Invitrogen, Eugene, Oregon) solution (1.25 μL Alexa-Fluor antibody in 1 mL 6% donkey serum blocking agent) for one hour at room temperature. Following incubation, the sample was again rinsed with 5 x 3 mL PBS aspirations and removed from the culture plate.

The sample was imaged with an FV-1000 confocal microscope (Olympus, Center Valley, Pennsylvania). Images were taken at the center of the disk and along three radial lines at each of the nine concentric circle intersections for a total of 27 images per disk. This constituted one (n=1) experiment. A 10x dry objective (Olympus, Center Valley,

Pennsylvania) was used to identify the location on the disk, and a 100x (Olympus, Center Valley, Pennsylvania) dry objective with a 0.95 numerical aperture and a 1 mm working distance was used to capture the images. The representative image shown in Figure 3.4.1 covered an area of 105.77 μm by 105.77 μm. For the raw platelet counts, statistical significance was determined using a Student's t-test (α=0.05).
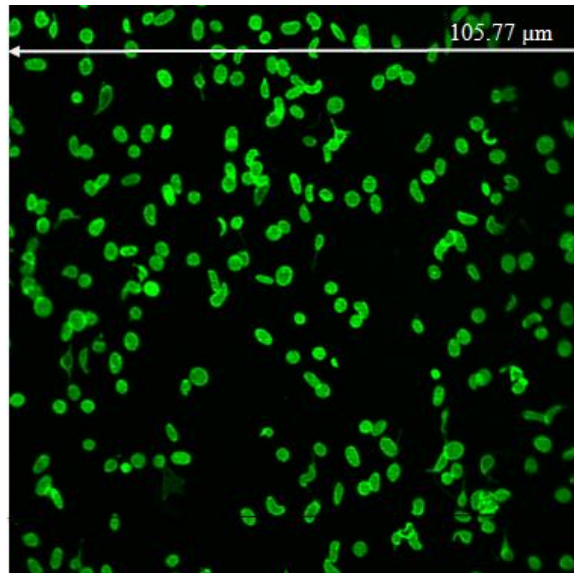
Figure 3.4.1 A representative confocal image taken at a radial intersection. The length of the scale bar is 105.77 μm.

3.5 Platelet Adhesion Measurements

Platelet adhesion was quantified using an adhesion coefficient (AC). This coefficient measures the ratio of the number of adhered platelets to the number of platelets transported to the PUU surface, and it is expressed as a percentage.(40) If none of the platelets that were transported to the surface adhered, the AC would be 0%, and if all of the platelets that were

transported to the surface adhered, the AC would be 100%. The AC was calculated as follows:

$$AC = 100\% \times \frac{N}{jt} \tag{37}$$

where N is the average number of platelets at an intersection per unit area, j is the platelet flux, and t is the rotation time.(40) The platelet flux, j, was calculated as follows:

$$j = \frac{0.62 D_{eff}{}^{2/3} \omega^{1/2} C_\infty}{\nu^{1/6}} \tag{38}$$

where D_{eff} is the effective diffusivity, ω is the angular velocity, C_∞ is the bulk platelet concentration, and ν is the kinematic viscosity.(40) In whole blood, the effective platelet diffusivity is defined as the total sum of the stationary flow diffusivity (D_{SF}) and the particle (D_p) diffusivity.(49)

$$D_{eff} = D_{SF} + D_p \tag{39}$$

For whole blood, the stationary flow diffusivity is a modified version of the Brownian diffusivity (D_f).(50) This modified version accounts for hematocrit, Φ, as follows:

$$D_{SF} = D_f \times \frac{1 - \phi}{1 + \dfrac{\phi}{1.05}} \tag{40}$$

Additionally, the Brownian diffusivity is calculated as follows:

$$D_f = \frac{K_B T}{6\pi\eta b} \qquad (41)$$

where K_B is the Boltzmann constant, T is the absolute temperature, η is the dynamic viscosity, and b is the average platelet radius.(40)   The particle diffusivity is defined as follows:

$$D_p = k\phi(1-\phi)^n a^2 \gamma \qquad (42)$$

where k and n are experimental constants, Φ is the hematocrit, a is the average red blood cell radius, and γ is the shear rate.(49)

Since whole blood is a non-Newtonian fluid, the viscosity varies with shear rate. Therefore, diffusivity and platelet flux were not constant for the entire disk; rather, these values changed along the disk radius. To determine the approximate viscosity values at each radial location, trendlines were fitted to the 20% Hct and 40% Hct experimental viscosity curves, shown in Figures 3.5.1 and 3.5.2. The asymptotic kinematic viscosities for the 20% Hct and 40% Hct reconstituted blood samples neared 2.7 cSt and 3.5 cSt, respectively.

y = -3E-06x + 0.0288
R² = 0.9474
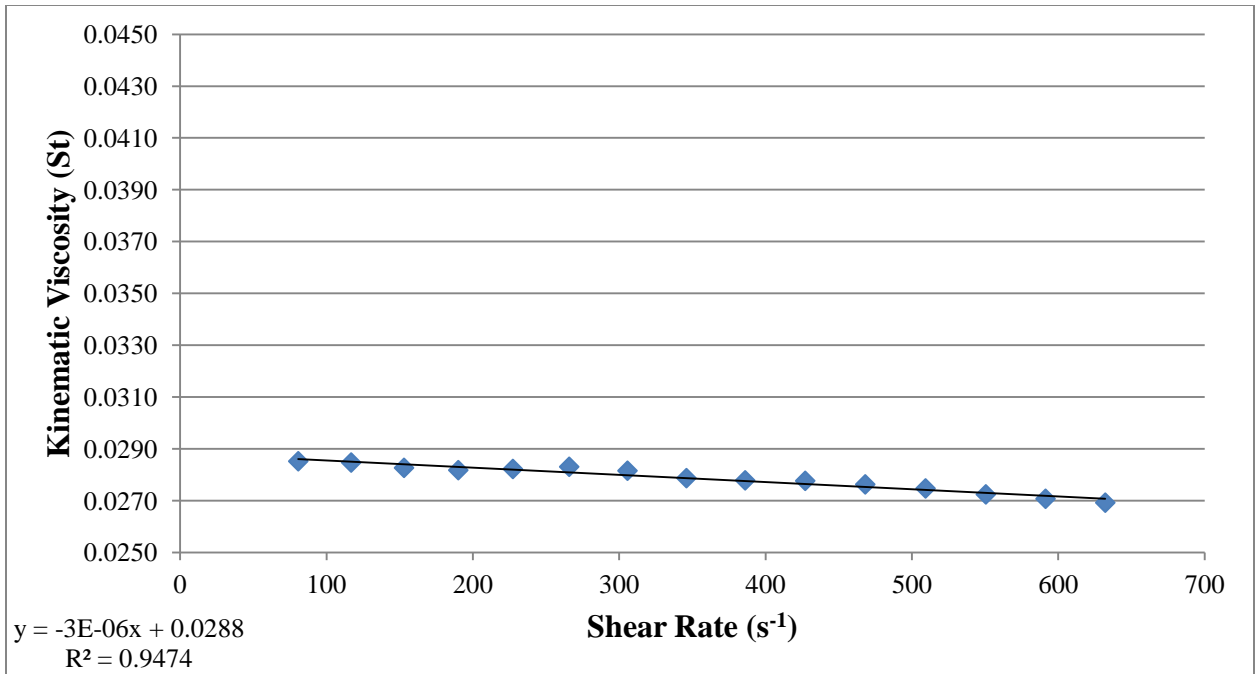
Figure 3.5.1 Experimental viscosity curve for 20% Hct reconstituted blood.

y = -0.002ln(x) + 0.0499
R² = 0.9881
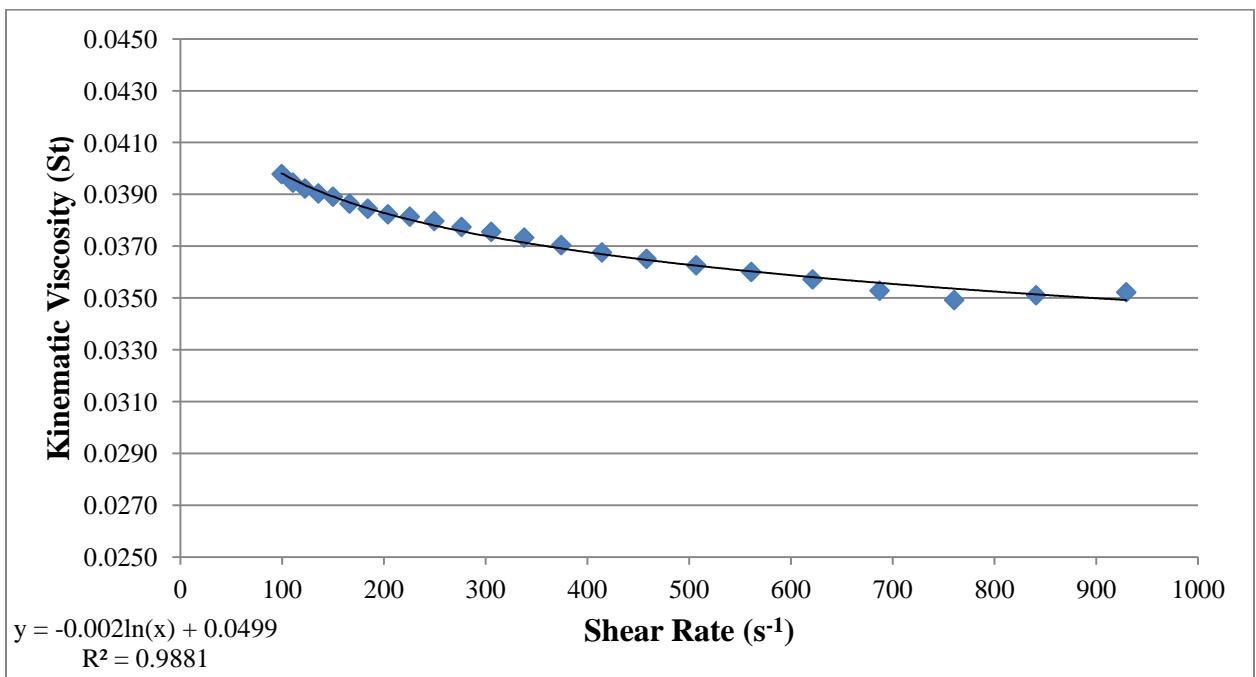
Figure 3.5.2 Experimental viscosity curve for 40% Hct reconstituted blood.

3.6 Shear Rate Measurements

Shear rates for both hematocrits were measured experimentally using laser Doppler velocimetry (LDV). LDV is a non-invasive optical imaging technique that is used to measure point velocities in a fluid using the Doppler effect. A thorough explanation of LDV theory is explained elsewhere.(51) Blood analogs were used to mimic the viscoelastic properties of the 20% and 40% Hct reconstituted blood samples. By weight, the 40% Hct blood analog was made of water (33.97%), glycerin (16%), sodium iodide (50%), and xanthan gum (0.03%). Similarly, the 20% Hct blood analog was made of water (34.991%), glycerin, (15%), sodium iodide (50%), and xanthan gum (0.009%). One component LDV was used to measure the radial velocities 100 μm beneath the disk surface. Ten thousand velocity measurements were made at each radial location, and data points +/- three standard deviations from the average were removed by filtering. Approximately 100 points at each radial location (or 1% of the data) were removed. Theoretical radial velocities at the disk surface were calculated using Equation 43.

$$v = \omega r \tag{43}$$

The shear rates, shown in Figures 3.5.3 and 3.5.4, were calculated by dividing the difference in velocity at the disk surface and 100 μm below the surface by the distance, 100 μm. For both 20% Hct and 40% Hct, shear rate varies linearly with radial distance from the disk center. The experimental shear values were used in the viscosity trendline equations to determine the viscosity at each location, and these values were used in the diffusivity and platelet flux calculations.

28

y = 85.408x + 24.182
R² = 0.9941
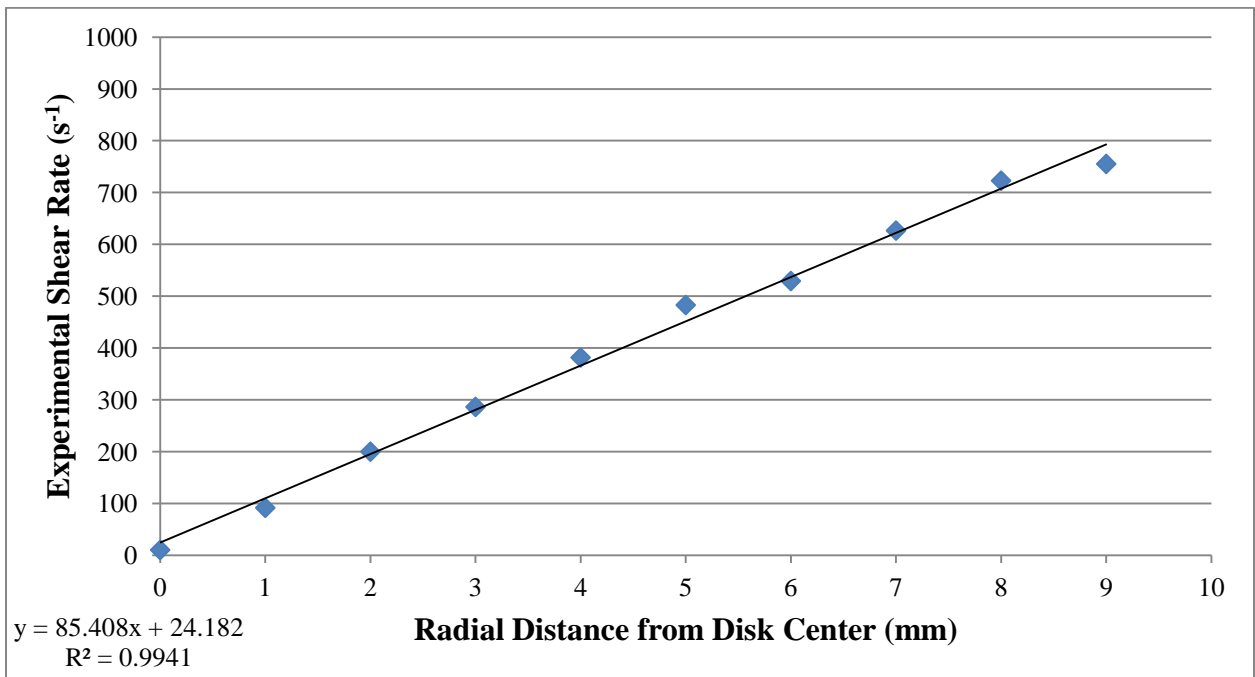
Figure 3.5.3 Experimental shear rate curve for 20% Hct reconstituted blood.

y = 95.839x - 50.4
R² = 0.9856
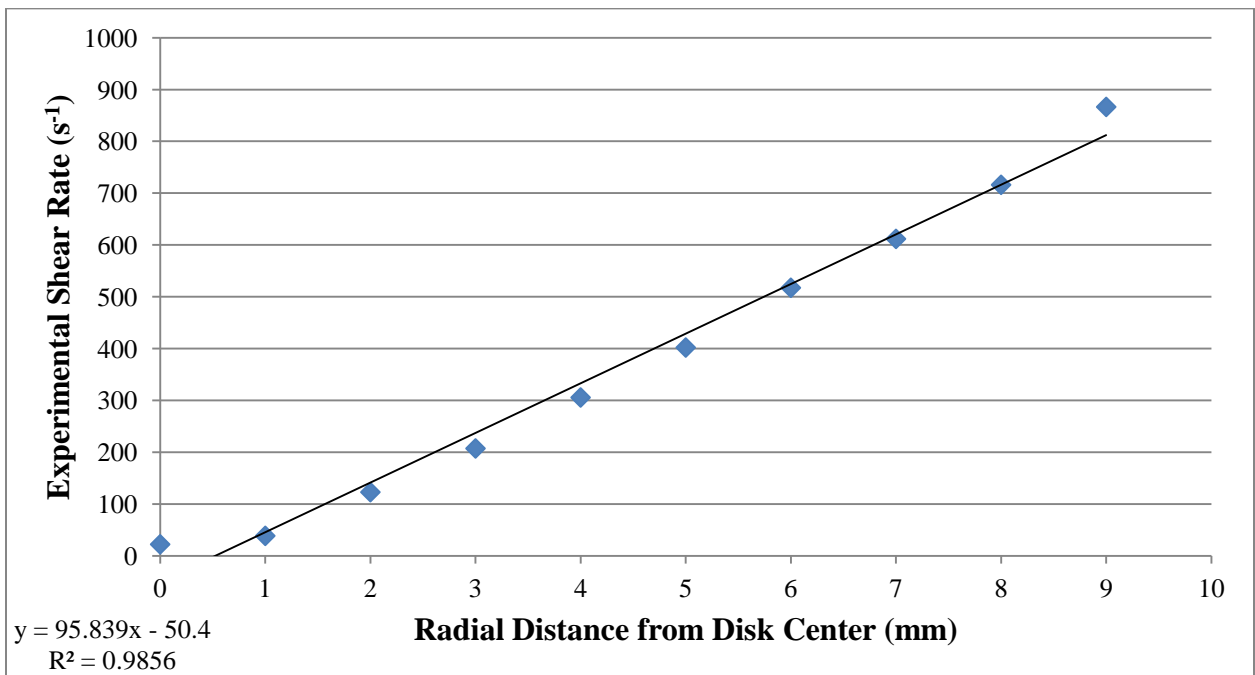
Figure 3.5.4 Experimental shear rate curve for 40% Hct reconstituted blood.

Chapter 4

Results and Discussion

4.1 Interpretation of Steady Rotation Experiments

In this study, our goal was to better understand platelet adhesion to PUU. PUU samples were mounted to the surfaces of 20 mm diameter disks and rotated in reconstituted whole bovine blood. Unlike the results from previous studies that used PRP as the fluid medium, our results account for the presence of red blood cells. In particular, we aimed to understand how hematocrit and rotation time affect platelet adhesion. Six (n=6) experiments were completed for each of the following experimental conditions: 20% Hct, 0.5 hour; 20% Hct, 1 hour; 20% Hct, 2 hour; 40% Hct, 0.5 hour; 40% Hct, 1 hour; and 40% Hct, 2 hour. In the following graphs, each data point represents the average platelet count at a radial location (with corresponding experimental shear rate) or a time point, and the error bars represent plus and minus one standard error of the mean (SEM). For all experiments, the SEMs are very large, suggesting the need for a greater number of experiments. Therefore, the data is analyzed by comparing the average values. Lastly, the data point furthest from the disk center is omitted in all graphs, as its value is influenced by edge effects. The raw data may be found in Appendix A.

4.2 Platelet Count vs. Shear Rate

The theoretical platelet fluxes, calculated using Equation 38, are shown in Figure 4.2.1. For both hematocrits, the platelet fluxes are lowest at the disk centers and increase logarithmically with shear rate. The platelet flux is greater for the 40% Hct blood than it is for the 20% Hct blood.
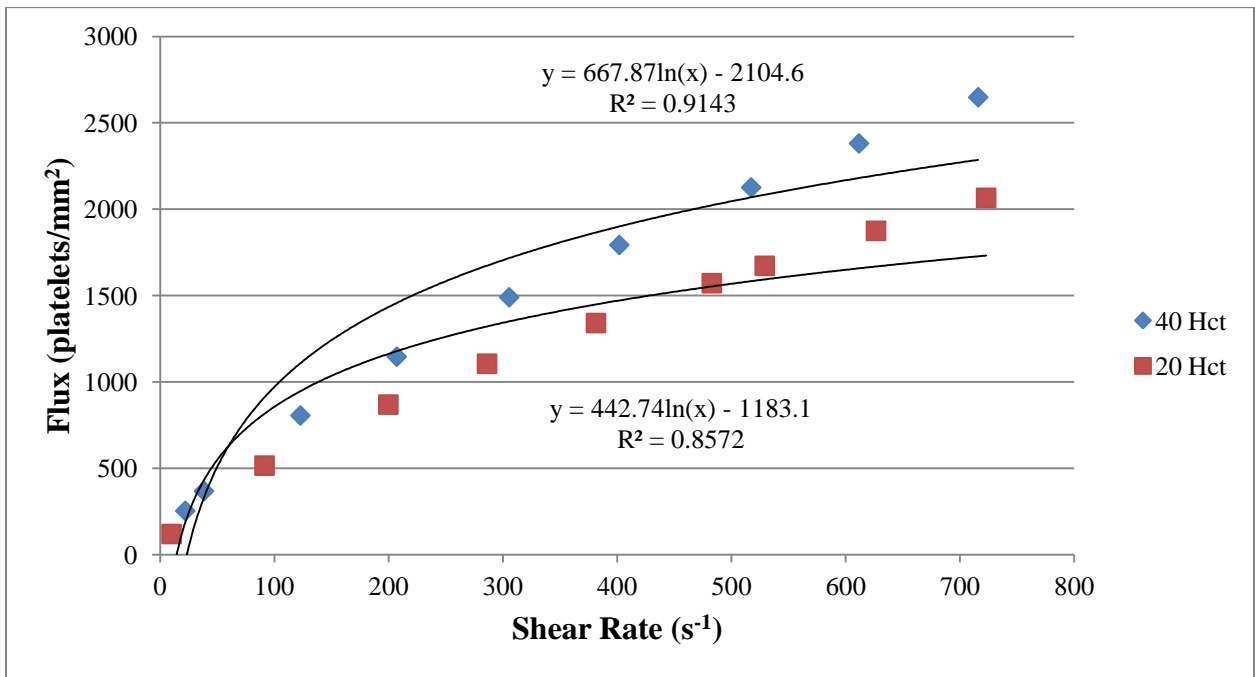
Figure 4.2.1 For both hematocrits, the platelet flux is lowest at the disk center and increases logarithmically with shear rate.

After imaging the disks, we manually counted and plotted the raw platelet numbers as a function of experimental shear rate. For all experimental conditions, the lowest average platelet count is at the disk center (except 40% Hct, 0.5 hour), and the relationship between platelet count and shear rate can be described by a logarithmic curve. The 40% Hct, 2 hour condition is shown in Figure 4.2.2. Above 200 s^{-1}, the average platelet count remains close to 150 platelets, regardless of the shear rate. No statistical significance is observed.

$y = 36.838\ln(x) - 71.817$
$R^2 = 0.9138$
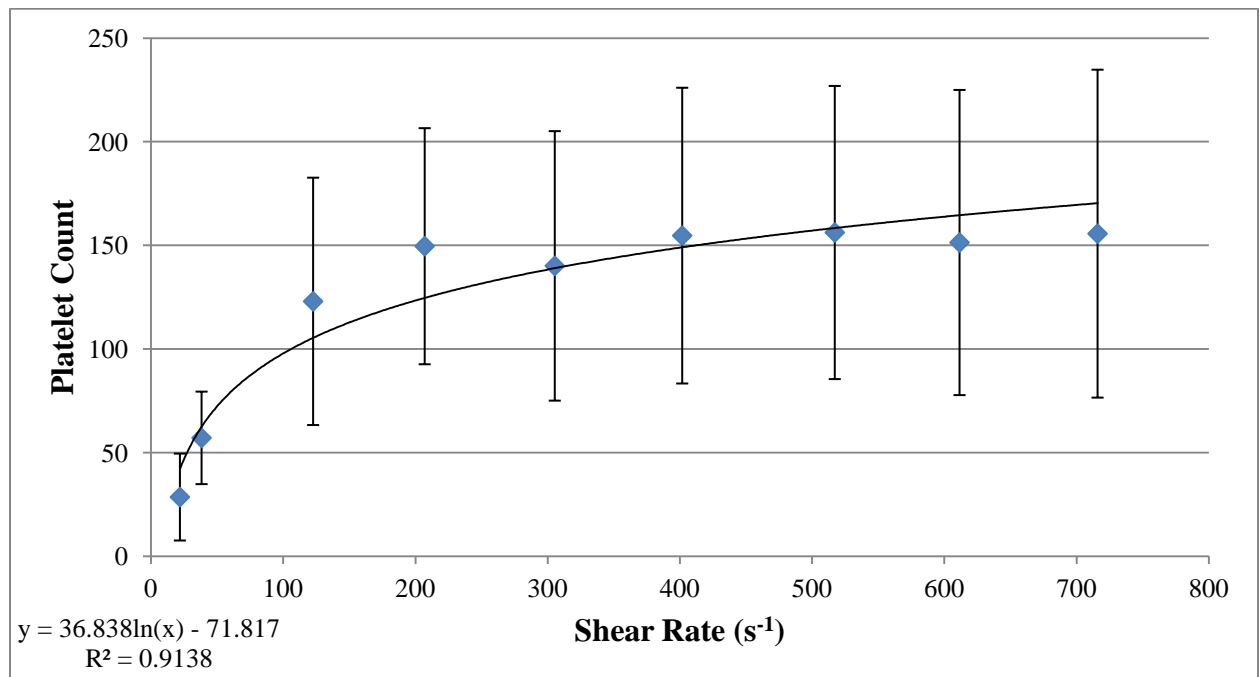
Figure 4.2.2 The 40% Hct, 2 hour condition shows the strongest logarithmic correlation between platelet count and shear rate.

A similar trend is observed for the 20% Hct, 2 hour condition, shown in Figure 4.2.3. However, at this condition, the platelet count does not reach a plateau until around 300 s^{-1}. Interestingly, beyond 300 s^{-1}, the platelet count remains close to 150 platelets, perhaps

indicating that the platelet-plasma protein binding kinetics limit adhesion. The platelet count at the disk center is statistically significant from all other locations.

$y = 37.925\ln(x) - 89.565$
$R^2 = 0.7486$
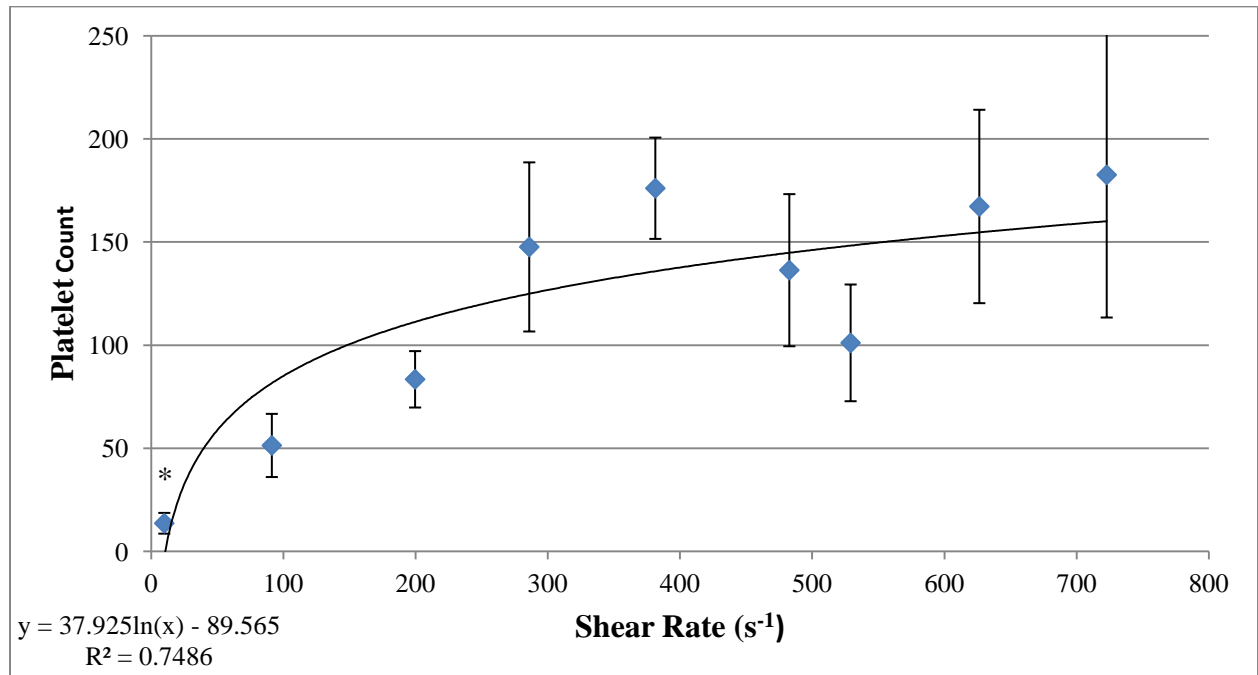
Figure 4.2.3 The 20% Hct, 2 hour condition shows a logarithmic trend similar to the 40% Hct, 2 hour condition. However, the 40% Hct, 2 hour condition reaches an asymptotic platelet count faster than the 20% Hct, 2 hour condition.

Therefore, at higher shear rates, the average platelet count does not vary between the two hematocrits after two hours of rotation. However, the 40% hematocrit reaches this plateau at a lower shear rate than the 20% hematocrit. This result is intuitive, as the presence of red blood cells is expected to increase platelet diffusivity and, consequently, platelet adhesion to the PUU surface. Therefore, in the 40% Hct blood, platelet diffusivity is maintained at lower shear rates due to the greater number of red blood cells.

33

At 0.5 hours, a similar relationship between the 20% Hct data and the 40% Hct data exists. As shown in Figure 4.2.4, the platelet counts are lowest at and near the disk center for both hematocrits, and at higher shear rates, they plateau. Again, the 40% Hct condition reaches its plateau at a lower shear rate (400 s^{-1}) than the 20% Hct condition (slightly above 500 s^{-1}), and the asymptotic platelet counts are similar for both hematocrits (about 20-35 platelets). For both hematocrits, the shear rates at which the platelet counts plateau are greater at 0.5 hours than at 2 hours.
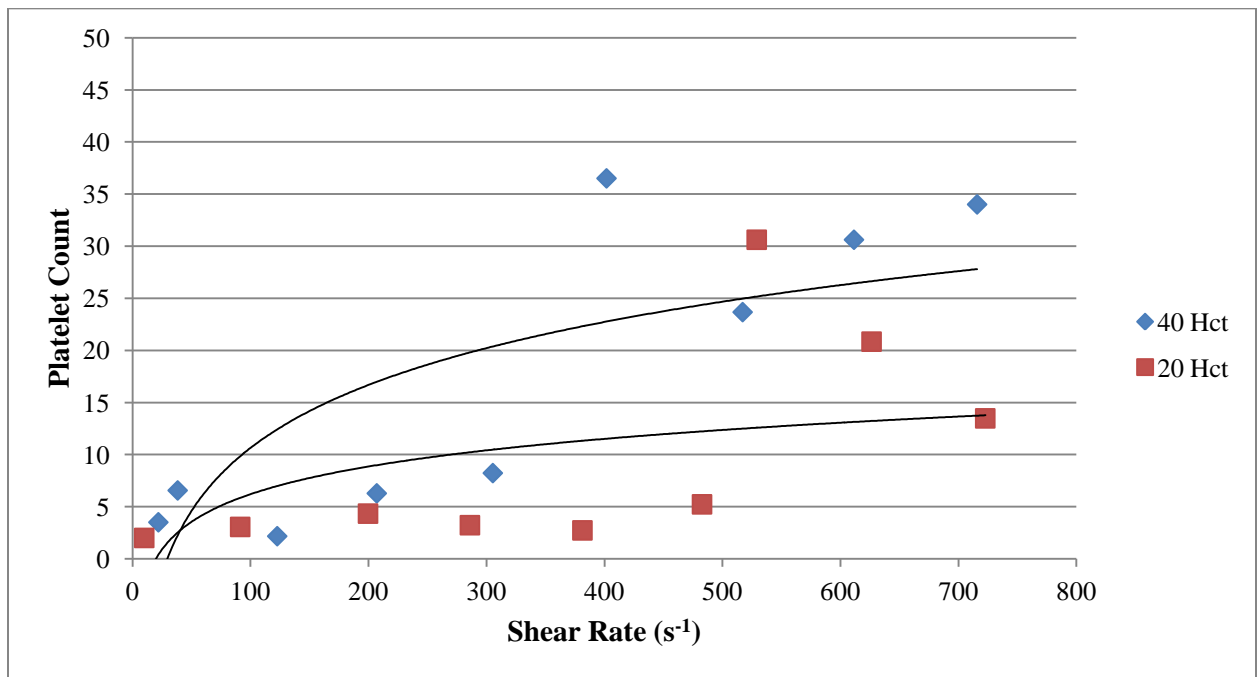
Figure 4.2.4 At 0.5 hours, both hematocrits have relatively low (<10 platelets) platelet counts before reaching an upper plateau. The 40% Hct condition reaches this upper plateau around 400 s^{-1}, and the 20% Hct condition reaches this upper plateau around 500 s^{-1}.

34

This trend, however, does not hold at 1 hour, as shown in Figure 4.2.5. The 20% Hct average platelet count plateaus around 80 platelets. The 40% Hct condition, however, stays relatively low for all of the radial positions. Only at one location (7 mm from the disk center) does the average platelet count exceed 20 platelets. This result is counterintuitive, as the higher hematocrit is expected to have greater platelet diffusivity and, consequently, more platelet adhesion due to the greater number of red blood cells. This result is thought to be due to the inherent variability in the data. Additional experiments should be done to further investigate whether or not platelet counts are truly higher for 20% Hct blood after one hour of rotation.
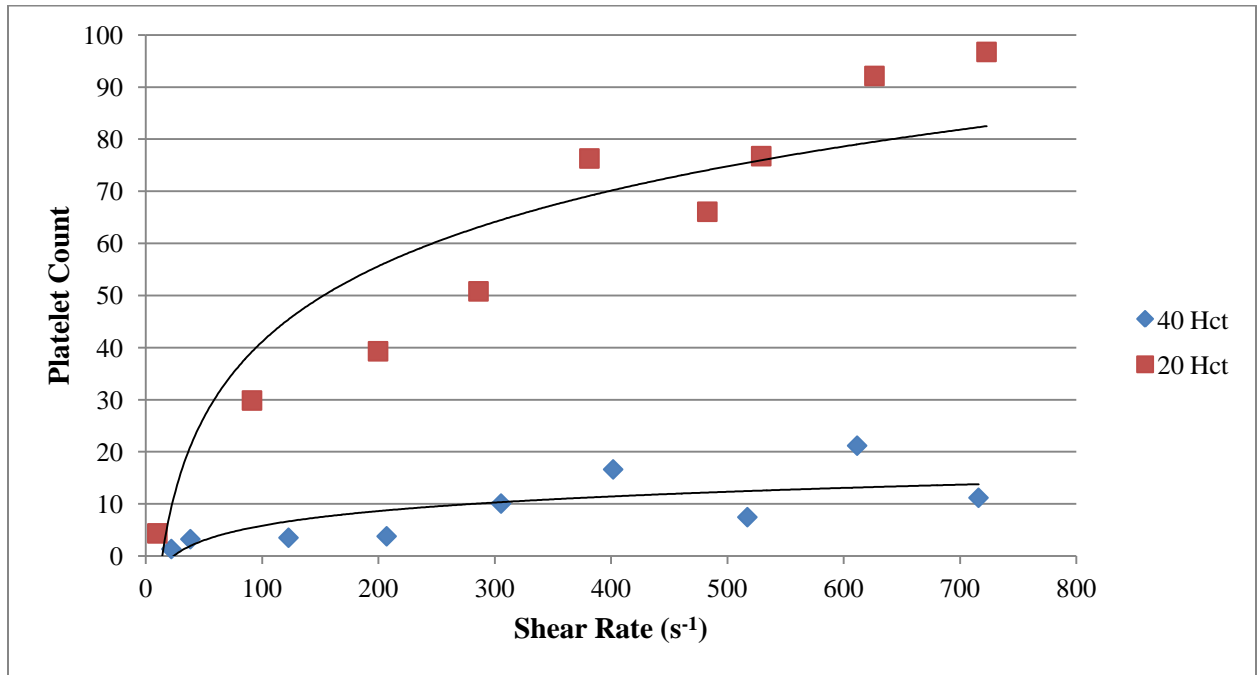
Figure 4.2.5 At 1 hour, the 20% Hct condition reaches a plateau of about 75 platelets. The 40% Hct condition, however, does not change much in the radial direction.

Figures 4.2.2-4.2.5 are contrasted with Figure 4.2.6, which shows the platelet counts after the PUU samples (n=6) were rotated in PRP for two hours.(41) We note that the image area (0.011187 mm^2) was the same for both the PRP and the whole blood experiments, so raw platelet counts provide an accurate comparison. The PRP experiments, however, had a higher platelet concentration (350×10^6 platelets/mL) than did the whole blood experiments (250×10^6 platelets/mL).(41) Unlike the whole blood experiments, the highest average platelet count for PRP is at the center of the disk, and the platelet count decays exponentially with increasing shear rate. Above 200 s^{-1}, the platelet count does not exceed 10 platelets.

$y = 21.401e^{-0.003x}$
$R^2 = 0.8902$
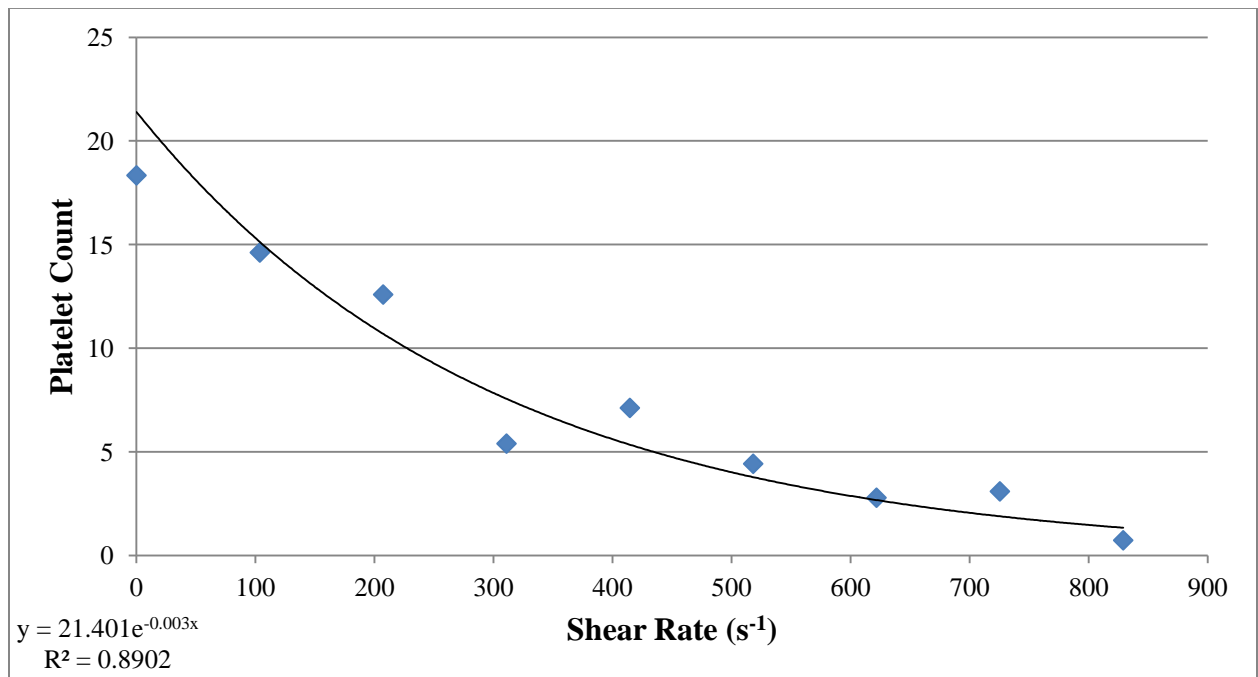
Figure 4.2.6 Platelet count versus shear rate for 2 hours, PRP. Platelet counts are highest at the disk center, decrease exponentially with shear rate, and are an order of magnitude less than the whole blood counts.(41)

The only difference between the two hour whole blood and PRP experiments, other than the presence of the red blood cells, is the increased platelet concentration in the PRP experiments. However, even with an increased platelet concentration, the platelet counts are much lower for the PRP experiments. Therefore, it is concluded that the red blood cells are responsible for the increased platelet counts. Specifically, they act through localized mixing, cell-cell collisions, platelet margination, or some combination of these physical mechanisms to increase platelet flux to the PUU surface.

4.3 Platelet Count vs. Time

The average platelet counts at each radial location were plotted against time for the 20% Hct (Figures 4.3.1-4.3.3) and 40% Hct (Figures 4.3.4-4.3.6) data. At each location, the platelet count increased linearly with time, a result that agrees with the literature.(52, 53) At all radial positions (except 6 mm) for the 20% Hct data, the R^2 value was greater than or equal to 0.94, indicating a strong linear correlation. For the 20% Hct data, the most gradual slope was at the disk center (m=0.0021), and the steepest slope was at 8 mm, the outermost radial location (m=0.0322).
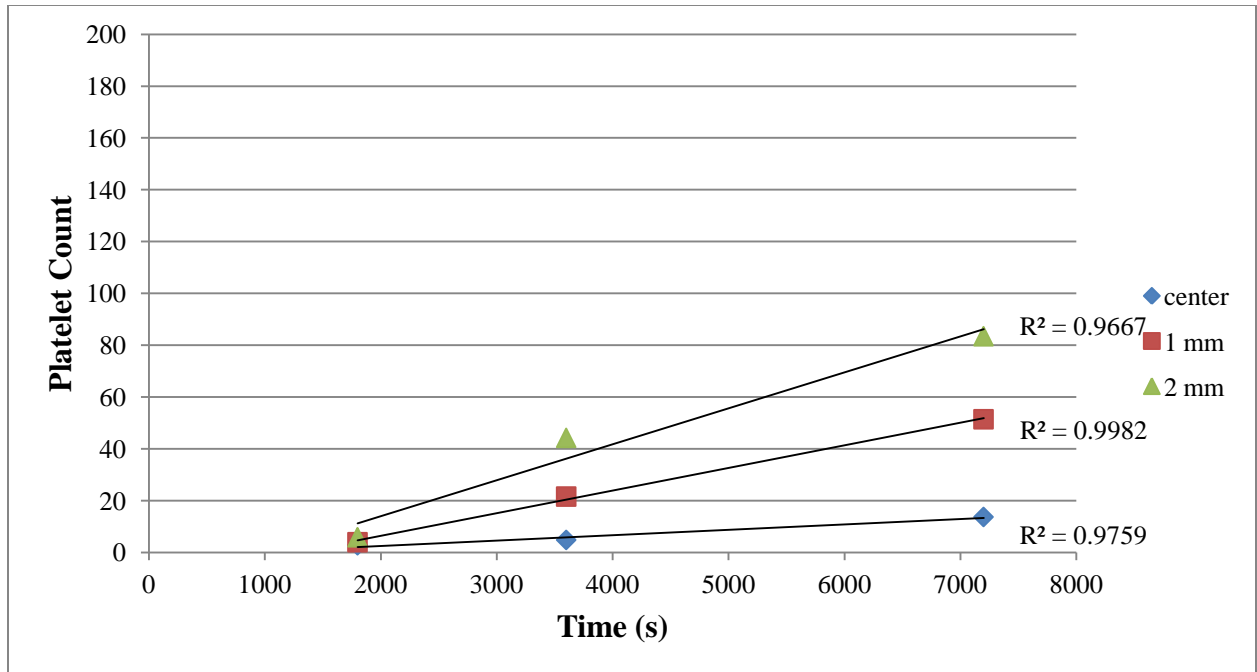
Figure 4.3.1 Average platelet counts at central, 1 mm, and 2 mm radial positions versus time for 20% Hct.
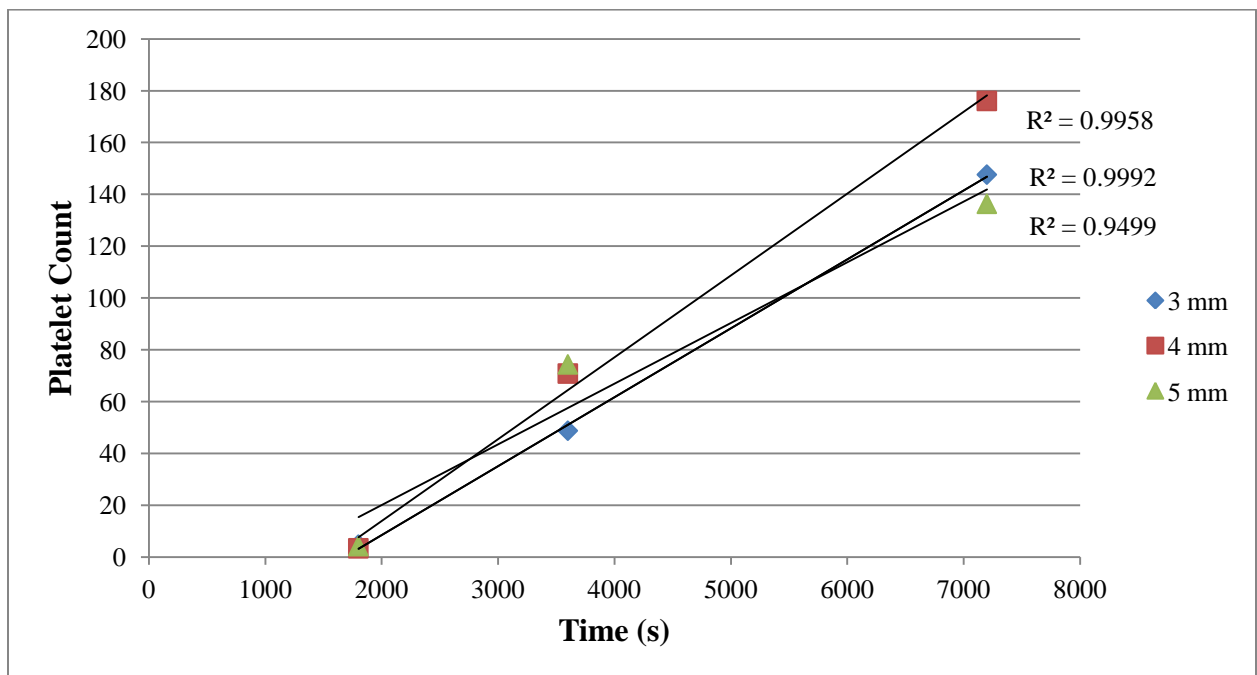
Figure 4.3.2 Average platelet counts at 3 mm, 4 mm, and 5 mm radial positions versus time for 20% Hct.
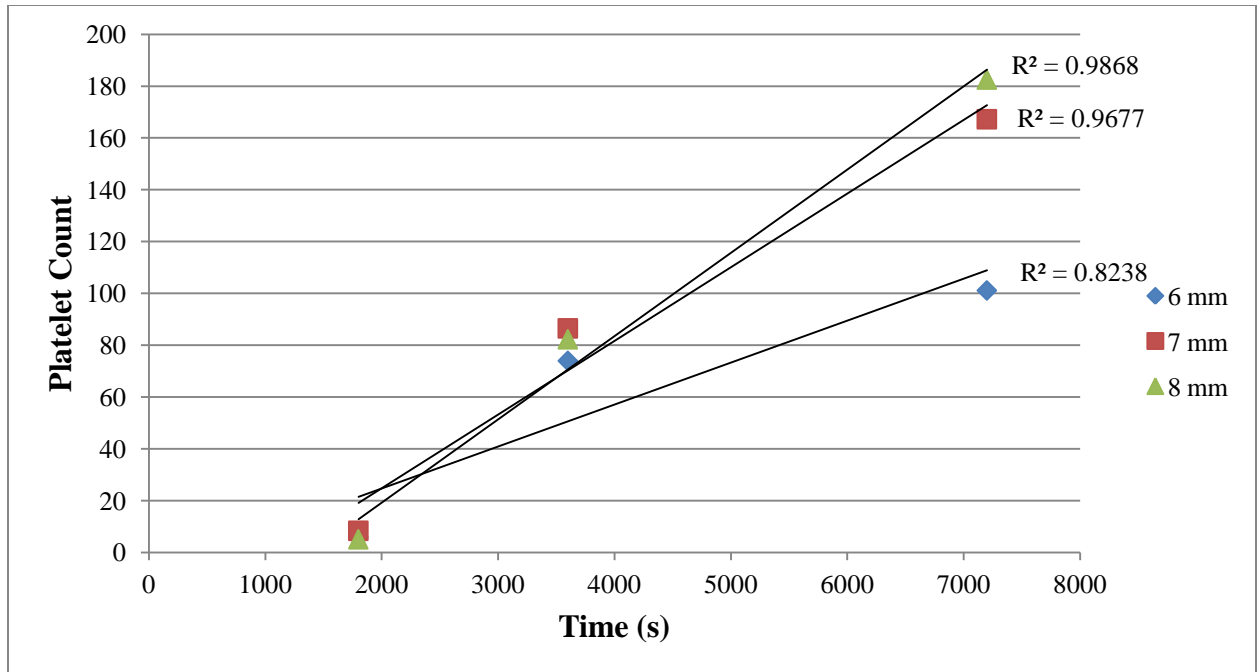
Figure 4.3.3 Average platelet counts at 6 mm, 7 mm, and 8 mm radial positions versus time for 20% Hct.

Due to the relatively low platelet counts for the 40% Hct, 1 hour condition, the linear relationships are not as strong for the 40% Hct data.
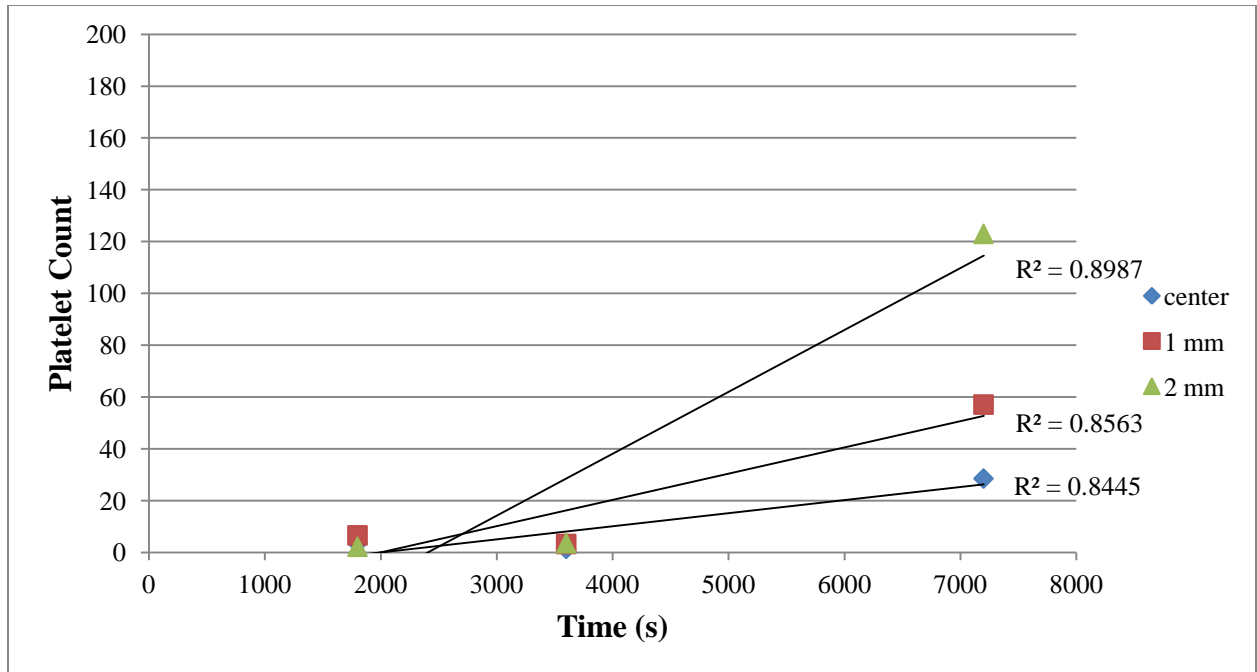
Figure 4.3.4 Average platelet counts at central, 1 mm, and 2 mm radial positions versus time for 40% Hct.
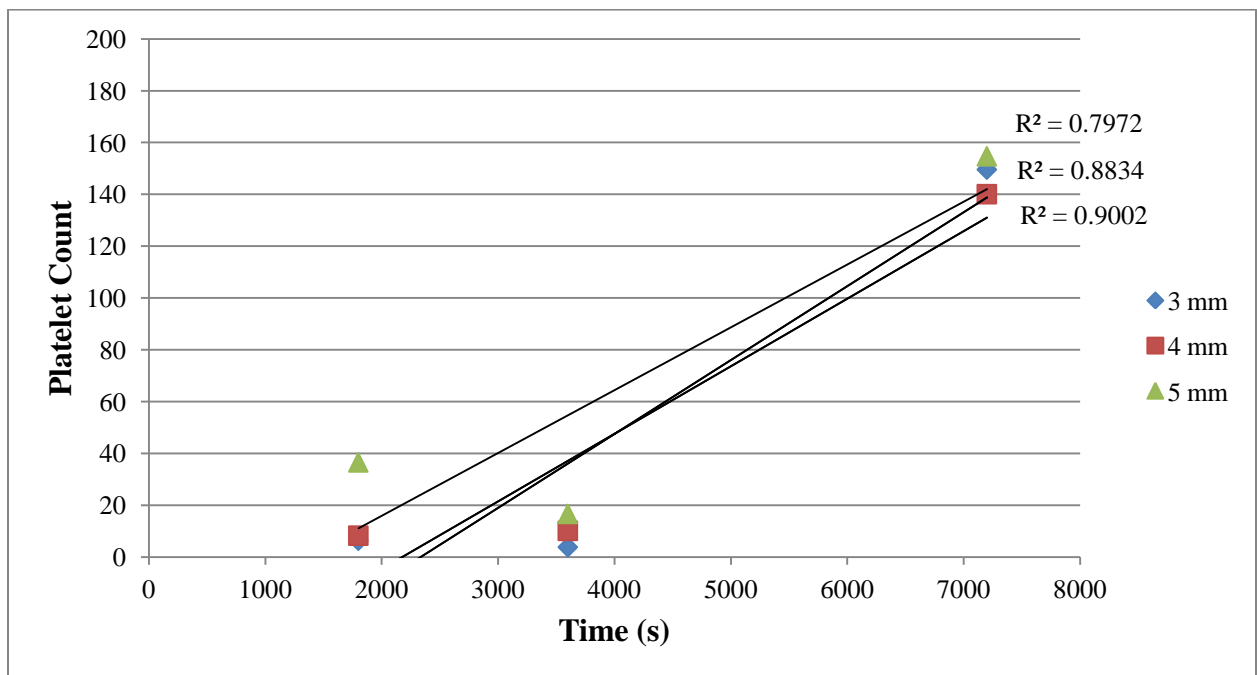
Figure 4.3.5 Average platelet counts at 3 mm, 4 mm, and 5 mm radial positions versus time for 40% Hct.

R² = 0.7859

R² = 0.8239

R² = 0.8494
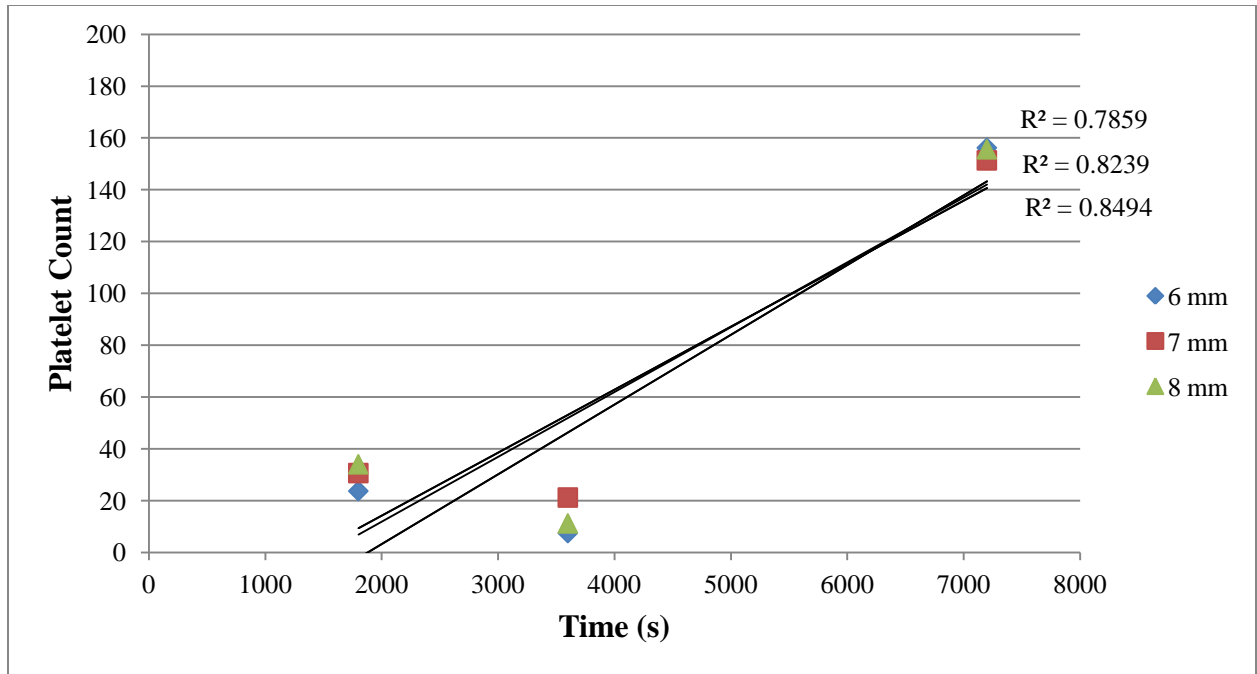
Figure 4.3.6 Average platelet count at 6 mm, 7 mm, and 8 mm radial positions versus time for 40% Hct.

4.4 Adhesion Coefficients

Zydney and Colton's diffusion equation (Equation 42) was developed by gathering data from numerous studies that measured the particle diffusivity, D_p, of deformable particles, such as liquid drops and red blood cells. The dimensionless particle diffusivities, $D_p/a^2\gamma$, from these experiments were plotted as a function of particle volume fraction (i.e. hematocrit) and were fit to a curve to yield Equation 42. The constants k (0.15 +/- 0.03) and n (0.8 +/- 0.3) were chosen such that the sums of the squared residuals were minimized. All of the data came from Couette or tube flow experiments.(49) Therefore, in order to use Equation 42 to calculate platelet diffusivity, we must assume that the physical mechanisms that lead to increased platelet diffusivity in Couette and tube flow are similar to those mechanisms that contribute to increased platelet diffusivity in flow due to a rotating disk.

41

There are two RBC shear-mediated mechanisms that increase platelet diffusivity: localized mixing and cell-cell collisions. Given their dependence on shear, it is necessary to compare how shear varies in Poiseuille flow, Couette flow, and flow due to a rotating disk in order to determine whether or not the above assumptions are accurate. In fully developed Poiseuille flow of a Newtonian fluid, the parabolic velocity profile remains constant along the length of the tube. Therefore, the wall shear stress also remains constant along the length of the tube. However, at the tube center, the shear rate is zero, and it increases linearly, reaching a maximum at the wall and creating a shear gradient in the radial direction. Conversely, in Couette flow, the shear stress remains constant in the entire fluid domain. In rotating disk flow, the shear rate increases linearly in the radial direction near the disk surface. Therefore, flow due to a rotating disk appears to be more similar to Poiseuille flow, in that both flows exhibit a radial shear gradient. It is possible that red blood cells behave similarly in these flows, as they are acted upon by varying degrees of shear. However, as Couette flow also showed increased platelet diffusivity in the absence of a shear gradient, it cannot be concluded that a shear gradient alone is responsible for these mechanisms. Rather, shear, which is described by the velocity gradient, is sufficient. The velocity profiles for Poiseuille flow (parabolic) and Couette flow (linear) are different. However, both flows result in increased platelet diffusivity. Therefore, it is concluded that rotating disk flow, which has a linear velocity gradient in the radial direction, will have the same RBC shear-induced effects as Poiseuille and Couette flow.

Platelet margination is a function of shear rate and hematocrit. Therefore, increases in hematocrit should theoretically result in increases in platelet diffusivity and, consequently, increased platelet adhesion. In this study, however, platelet adhesion was relatively similar

for both the 20% Hct and 40% Hct hematocrits. Therefore, it is concluded that platelet margination either does not occur, or platelet margination occurs to such a small degree that it is insignificant. This is consistent with Zydney and Colton's analysis, which concluded that shear dependent mechanisms (localized mixing and cell-cell collisions) had the most significant effect on platelet diffusivity.(49) Thus, this result is in agreement with their conclusions. Based on the above reasoning, it is concluded that the same physical RBC mechanisms in Poiseuille and Couette flow are responsible for increased platelet diffusivity in rotating disk flow. Therefore, the particle diffusivity described by Zydney and Colton is accurate.

Figures 4.4.1 and 4.4.2 show the adhesion coefficient as a function of shear rate for both the 20% Hct and 40% Hct conditions after 2 hours of rotation. The adhesion coefficients are plotted with the average k and n values (blue diamonds) and the combinations of k and n that produce the maximum (red squares) and minimum (green triangles) particle diffusivities. The adhesion coefficient decreases exponentially with increasing shear rate for both hematocrits, but the 40% Hct data has a much stronger correlation. The maximum adhesion coefficient for 20% Hct occurs at the disk center and is approximately 0.15%. The maximum adhesion coefficient for 40% Hct also occurs at the disk center and is approximately 0.20%. Adhesion coefficient graphs for 0.5 and 1 hours are included in Appendix A, as there are no trends for discussion.
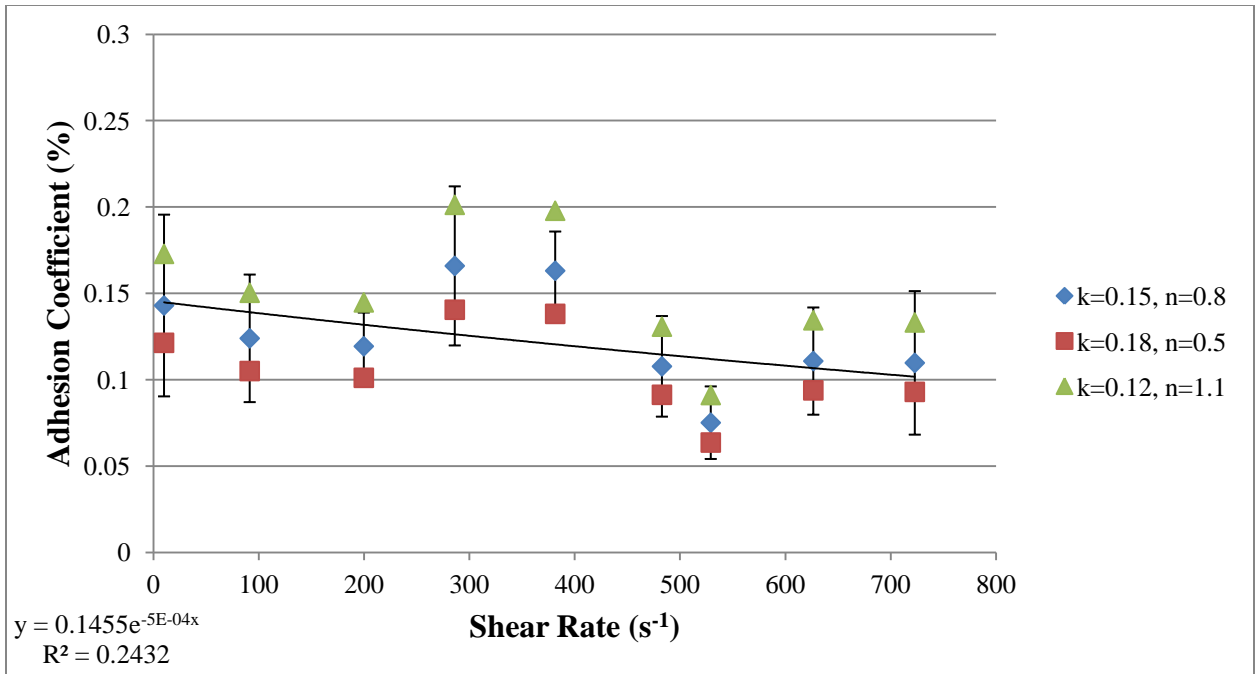
Figure 4.4.1 Adhesion coefficient versus shear rate for 20% Hct, 2 hours.
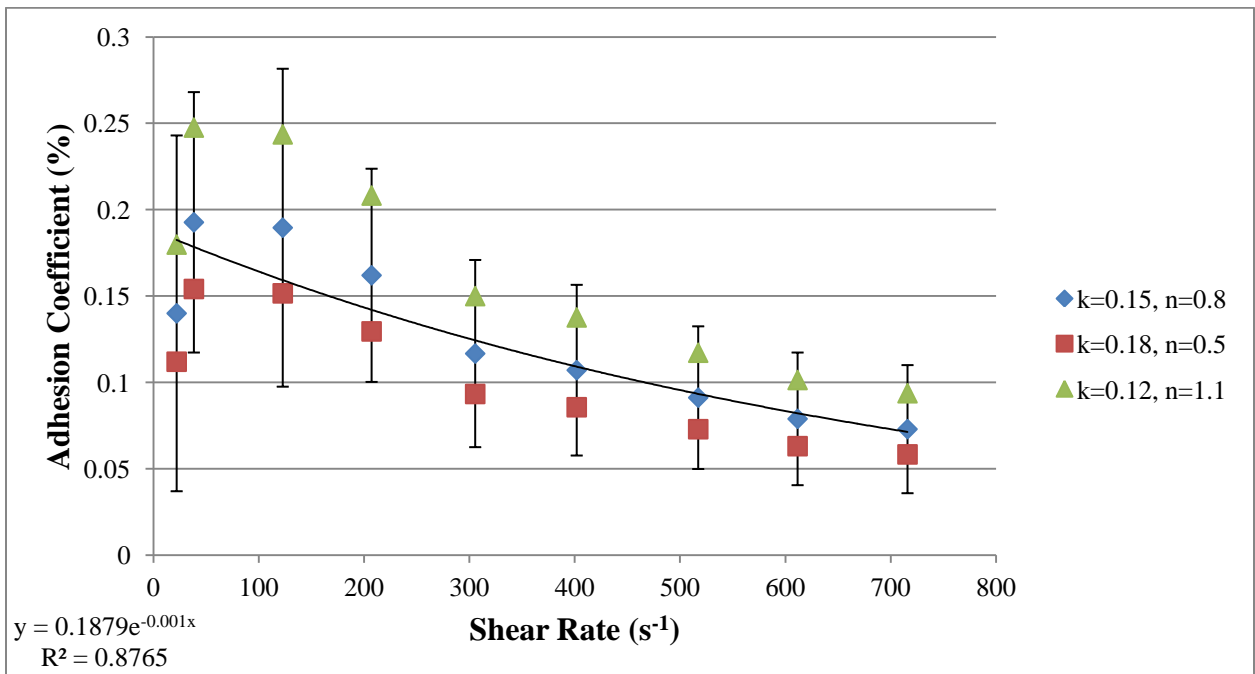
Figure 4.4.2 Adhesion coefficient versus shear rate for 40% Hct, 2 hours.

The adhesion coefficient data for the PRP experiments is shown in Figure 4.4.3. The maximum adhesion coefficient occurs at the disk center, as it does in the whole blood experiments, and it is approximately 0.70%. This result is surprising, however, as even though the number of platelets adhered is much lower for PRP, the adhesion coefficient is much greater. This difference is due to the diffusion coefficient calculation. As PRP effectively has a 0% Hct, the particle diffusivity term drops out of the diffusivity calculation, and the only term that remains is the Brownian diffusivity. Brownian diffusivity is orders of magnitude smaller than particle diffusivity, so the platelet flux is also order of magnitude smaller for the PRP experiments. When calculating the adhesion coefficient, you must divide by the flux. Therefore, you divide by a much smaller number for the PRP experiments. Although the number of platelets per unit area (a term in the numerator of the adhesion coefficient) is an order of magnitude greater for whole blood, this does not compensate for the platelet flux that is multiple orders of magnitude smaller. Therefore, a larger adhesion coefficient for PRP is the result.
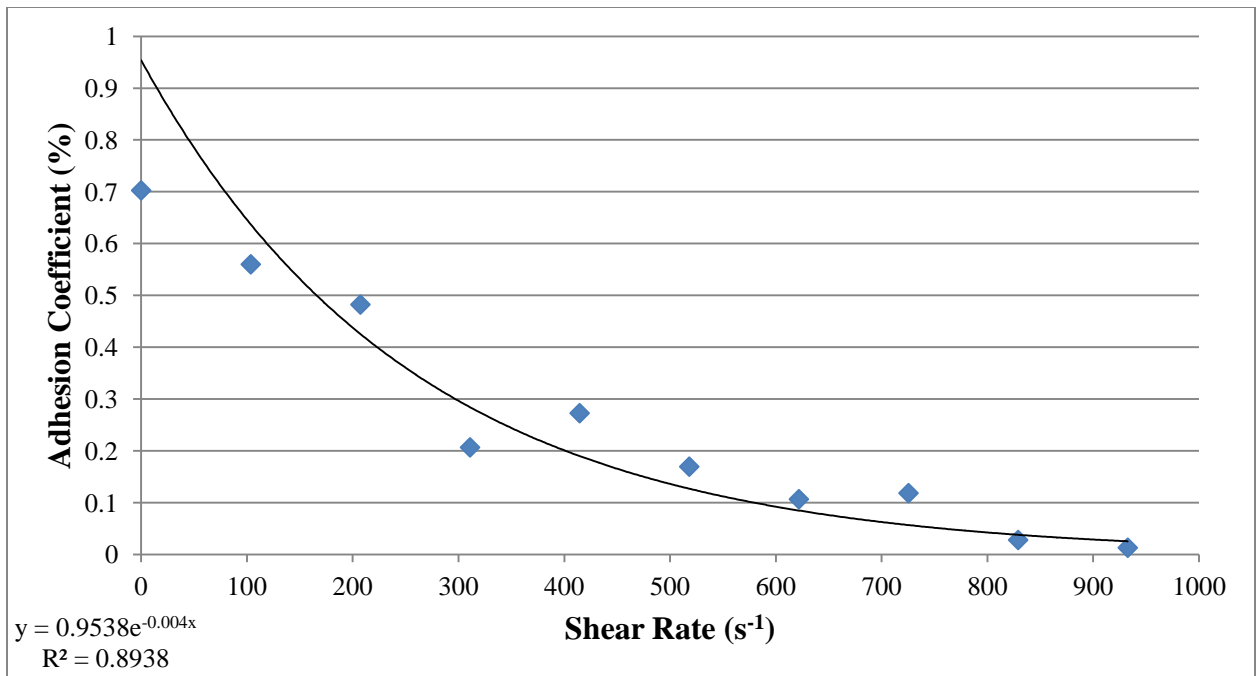
Figure 4.4.3 Adhesion coefficient versus shear rate for PRP, 2 hours.

Chapter 5

Conclusions

5.1 Summary of Results

One of the most important conclusions from this work is that the presence of red blood cells greatly increases the number of platelets adhered to the PUU surface after rotation. Although the RBCs do not affect the actual binding of the platelets to the adsorbed plasma proteins, they increase the transport of the platelets to the plasma proteins, making them more readily available for binding. Because the number of adhered platelets was an order of magnitude greater in the whole blood experiments than it was in the PRP experiments, it will be important to use whole blood in any future experiments to more accurately study platelet adhesion.

Secondly, the results from this study demonstrate that increases in shear rate and rotation time have a greater effect on the number of adhered platelets than increases in hematocrit. The platelet count versus shear rate data demonstrate that the raw number of platelets adhered to the PUU surface increases logarithmically with increasing shear rate. This trend is mirrored by the platelet flux data, which show logarithmic increases in platelet flux with increasing shear rate. Additionally, the platelet count versus shear rate data show that increasing the hematocrit from 20% to 40% does not drastically increase the number of adhered platelets, as both conditions reached similar plateau platelet counts at higher shear rates for 0.5 and 2 hours. Although there is a difference at 1 hour, this is thought to be due to variability in the data. Because increasing hematocrit does not increase platelet adhesion, it is concluded that platelet margination either does not occur or that it occurs to such a small

degree that its effects are insignificant. Rather, increased platelet adhesion is a function of shear only, suggesting that localized RBC mixing and cell-cell collisions are responsible for increased platelet adhesion. Lastly, the platelet count versus time data demonstrate that the raw number of platelets adhered to the PUU surface increases linearly with rotation time.

5.2 Future Studies

Due to the variability in all of the data, one option for a future study would be to repeat the experiments in order to more soundly determine the trends. This will be especially important for the 40 Hct, 1 hour data, which showed lower numbers of adhered platelets compared to the 20% Hct condition. It is estimated that approximately nine (n=9) studies will be needed to detect a difference of 75 platelets with a standard deviation of 50 and a power of 0.85. Also, since the Penn State 50 cc device is a pulsatile VAD, another option for a future study is to use a pulsatile, rather than steady, waveform. Future studies should also be done to support the reasoning that the Zydney and Colton diffusion calculation is appropriate for the rotating disk. This will likely require experimentally measuring that diffusivities or determining how the red blood cells behave in the flow field using an optical imaging technique. Furthermore, it should be determined whether platelet adhesion is solely a function of physical parameters, such as shear rate, or whether chemical parameters also influence platelet adhesion. It would be interesting to determine whether the adhered platelets were also activated. If activated, then it is possible that factors other than shear rate, hematocrit, and rotation time, such as platelet-platelet interactions and the secretion of bulk phase agonists and coagulation cascade cofactors, are responsible for platelet adhesion.

REFERENCES

1. Roger VL, Go AS, Lloyd-Jones DM, Benjamin EJ, Berry JD, Borden WB, Bravata DM, et al. 2012. Heart disease and stroke statistics--2012 update: a report from the American Heart Association. *Circulation* 125(1):e2–e220.

2. Stehlik J, Edwards LB, Kucheryavaya AY, Benden C, Christie JD, Dobbels F, Kirk R, Rahmel AO, and Hertz MI. 2011. The Registry of the International Society for Heart and Lung Transplantation: Twenty-eighth Adult Heart Transplant Report--2011. *The Journal of Heart and Lung Transplantation* 30(10):1078–94. Elsevier Inc.

3. 2012. National Heart Lung and Blood Institute.

4. 2004. Organ Procurement and Transplantation Network.

5. Poirier VL. 1997. The heartmate left ventricular assist system: worldwide clinical results. *European Journal of Cardio-Thoracic Surgery* 11(97):S39–44.

6. Rose EA, Gelijns AC, Moskowitz AJ et al. 2001. Randomized Evaluation of Mechanical Assistance for the Treatment of Congestive Heart Failure (REMATCH) Study Group. Long-term mechanical left ventricular assistance for end-stage heart failure. *The New England Journal of Medicine* 345(20):1435–1443.

7. Lietz K, Long JW, Kfoury AG, Slaughter MS, Silver M a, Milano C a, Rogers JG, Naka Y, Mancini D, and Miller LW. 2007. Outcomes of left ventricular assist device implantation as destination therapy in the post-REMATCH era: implications for patient selection. *Circulation* 116(5):497–505.

8. Deng MC, Ardehali A, Shemin R, Hickey A, MacLellan WR, and Fonarow G. 2011. Relative roles of heart transplantation and long-term mechanical circulatory support in contemporary management of advanced heart failure - a critical appraisal 10 years after REMATCH. *European Journal of Cardio-Thoracic Surgery* 40(4):781–2.

9. Pierce W and Brighton J. 1974. Complete left ventricular bypass with a paracorporeal pump: Design and evaluation. *Annals of Surgery* 180(4):418–426.

10. Gaines WE, Pierce WS, Donachy JH, Rosenberg G, Landis DL, Richenbacher WE, and Waldhausen J a. 1985. The Pennsylvania State University paracorporeal ventricular assist pump: optimal methods of use. *World Journal of Surgery* 9(1):47–53.

11. Weiss W and Rosenberg G. 1990. Permanent circulatory support systems at the Pennsylvania State University. *IEEE Transactions on Biomedical Engineering* 37(2):138–145.

12. Bachmann C, Hugo G, Rosenberg G, Deutsch S, Fontaine A, and Tarbell JM. 2000. Fluid dynamics of a pediatric ventricular assist device. *Artificial Organs* 24(5):362–72.

13. Mehta SM, Pae WE, Rosenberg G, Snyder a J, Weiss WJ, Lewis JP, Frank DJ, Thompson JJ, and Pierce WS. 2001. The LionHeart LVD-2000: a completely implanted left ventricular assist device for chronic circulatory support. *The Annals of Thoracic Surgery* 71(3):S156–61; S183–4.

14. Mehta SM, Weiss WJ, Snyder a J, Prophet G a, Pae WE, Rosenberg G, and Pierce WS. 2000. Testing of a 50 cc stroke volume completely implantable artificial heart: expanding chronic mechanical circulatory support to women, adolescents, and small stature men. *ASAIO Journal* 46(6):779–82.

15. Yamanaka H, Rosenberg G, Weiss WJ, Snyder AJ, Zapanta CM, Pae WE, and Siedlecki CA. 2003. Multiscale Surface Evaluation of Thrombosis in Left Ventricular Assist Systems. *ASAIO Journal* 49(2):222.

16. Hochareon P, Manning KB, Fontaine A a., Tarbell JM, and Deutsch S. 2004. Correlation of In Vivo Clot Deposition With the Flow Characteristics in the 50 cc Penn State Artificial Heart: A Preliminary Study. *ASAIO Journal* 50(6):537–542.

17. Oley L a, Manning KB, Fontaine A a, and Deutsch S. 2005. Off-design considerations of the 50cc Penn State Ventricular Assist Device. *Artificial Organs* 29(5):378–86.

18. Kreider JW, Manning KB, Oley L a, Fontaine A a, and Deutsch S. 2006. The 50cc Penn State left ventricular assist device: a parametric study of valve orientation flow dynamics. *ASAIO Journal* 52(2):123–31.

19. Nanna JC, Wivholm J a, Deutsch S, and Manning KB. 2011. Flow field study comparing design iterations of a 50 cc left ventricular assist device. *ASAIO Journal* 57(5):349–57.

20. Navitsky M a, Deutsch S, and Manning KB. 2013. A thrombus susceptibility comparison of two pulsatile Penn State 50 cc left ventricular assist device designs. *Annals of Biomedical Engineering* 41(1):4–16.

21. Willians DF. 1987. Definitions in Biomaterials. In *Proceedings of a Consensus Conference of the European Society for Biomaterials*.

22. Willians DF. 1988. A model for biocompatibility and its evaluation. In *28th Annual Scientific Meeting of the Biological Engineering Society*.

23. Sastri VR. 2010. *Plastics in Medical Devices: Properties, Requirements and Applications*. 140–148.

24.   Hanson SR. 1993. Device thrombosis and thromboembolism. *Cardiovascular Pathology* 2(3):157–165.

25.   Gartner MJ, Wilhelm CR, Gage KL, Fabrizio MC, and Wagner WR. 2000. Modeling flow effects on thrombotic deposition in a membrane oxygenator. *Artificial Organs* 24(1):29–36.

26.   Milner KR, Snyder AJ, and Siedlecki C a. 2006. Sub-micron texturing for reducing platelet adhesion to polyurethane biomaterials. *Journal of Biomedical Materials Research* 76(3):561–70.

27.   Chiras D. 2012. *Human Biology*. 139.

28.   George JN. 2000. Platelets. *The Lancet* 355(9214):1531–1539.

29.   Grunkemeier JM, Tsai WB, McFarland CD, and Horbett T a. 2000. The effect of adsorbed fibrinogen, fibronectin, von Willebrand factor and vitronectin on the procoagulant state of adherent platelets. *Biomaterials* 21(22):2243–52.

30.   Uri M. 2010. Bionumbers: The Database of Useful Biological Numbers.

31.   Holme PA, Orvin U, Hamers MJ, Solum NO, Brosstad FR, Barstad RM, and Sakariassen KS. 1997. Shear-Induced Platelet Activation and Platelet Microparticle Formation at Blood Flow Conditions as in Arteries With a Severe Stenosis. *Arteriosclerosis, Thrombosis, and Vascular Biology* 17:646–653.

32.   Noh H and Vogler E a. 2006. Volumetric interpretation of protein adsorption: mass and energy balance for albumin adsorption to particulate adsorbents with incrementally increasing hydrophilicity. *Biomaterials* 27(34):5801–12.

33.   Roach P, Farrar D, and Perry CC. 2005. Interpretation of protein adsorption: surface-induced conformational changes. *Journal of the American Chemical Society* 127(22):8168–73.

34.   Tanaka M, Motomura T, Kawada M, Anzai T, Kasori Y, Shiroya T, Shimura K, Onishi M, and Mochizuki a. 2000. Blood compatible aspects of poly(2-methoxyethylacrylate) (PMEA)--relationship between protein adsorption and platelet adhesion on PMEA surface. *Biomaterials* 21(14):1471–81.

35.   Camacho a and Dimsdale JE. 2000. Platelets and psychiatry: lessons learned from old and new studies. *Psychosomatic medicine* 62(3):326–36.

36.   Hubbell JA and McIntire L V. 1986. Visualization and analysis of mural thrombogenesis on collagen, polyurethane and nylon. *Biomaterials* 7(5):354–360.

37.   Von Karman T. 1921. Uber laminare and turbulente Reibung. *Mathematik und Mechanik* 1:233–252.

38.   Cochran WG and Goldstein S. 2008. The flow due to a rotating disc. *Mathematical Proceedings of the Cambridge Philosophical Society* 30(03):365.

39.   Benton ER. 2006. On the flow due to a rotating disk. *Journal of Fluid Mechanics* 24(04):781.

40.   Wang I, Anderson JM, and Marchant RE. 1993. Adhesion to Hydrophobic Biomedical Polymer Is epidermidis Staphylococcus Mediated by Platelets. *The Journal of Infectious Disease* 167(2):329–336.

41.   Navitsky MA. 2012. *A Comparison of Thrombus Susceptibility for Two Pulsatile 50 cc Left Ventricular Assist Device*.

42.   Turitto VT and Baumgartner HR. 1975. Platelet deposition on subendothelium exposed to flowing blood: mathematical analysis of physical parameters. *ASAIO Journal* 21:593–601.

43.   Keller KH. 1971. Effect of fluid shear on mass transport in flowing blood. In *Federation*, pp. 1591–1599.

44.   Aarts P a., Van den Broek S a., Prins GW, Kuiken GD, Sixma JJ, and Heethaar RM. 1988. Blood platelets are concentrated near the wall and red blood cells, in the center in flowing blood. *Arteriosclerosis, Thrombosis, and Vascular Biology* 8(6):819–824.

45.   Yeh C and Eckstein EC. 1994. Transient lateral transport of platelet-sized particles in flowing blood suspensions. *Biophysical Journal* 66(5):1706–16.

46.   Karino T and Goldsmith HL. 1979. Adhesion of human platelets to collagen on the walls distal to a tubular expansion. *Microvascular Research* 17(3):238–262.

47.   Jordan a, David T, Homer-Vanniasinkam S, Graham a, and Walker P. 2004. The effects of margination and red cell augmented platelet diffusivity on platelet adhesion in complex flow. *Biorheology* 41(5):641–53.

48.   Rodefeld MD, Frankel SH, and Giridharan G a. 2011. Cavopulmonary assist: (em)powering the univentricular fontan circulation. *Seminars in Thoracic and Cardiovascular Surgery: Pediatric Cardiac Surgery Annual* 14(1):45–54. Elsevier Inc.

49.   Zydney AL and Colton CK. 1988. Augmented Solute Transport in the Shear Flow of a Concentrated Suspension. *PhysicoChemical Hydrodynamics* 10(1):77–96.

50. Wang N-HL and Keller K. 1985. Augmented transport of extracellular solutes in concentrated erythrocyte suspensions in couette flow. *Journal of Colloid and Interface Science* 103(1):210–225.

51. Albrecht HE, Borys M, Damaschke N, and Tropea C. 2003. *Laser Doppler and Phase Measurement Techniques*. 1–660.

52. Turitto VT and Baumgartner HR. 1975. Platelet interaction with subendothelium in a perfusion system: physical role of red blood cells. *Microvascular Research* 9(3):335–44.

53. Moroi M, Jung SM, Shinmyozu K, Tomiyama Y, Ordinas a, and Diaz-Ricart M. 1996. Analysis of platelet adhesion to a collagen-coated surface under flow conditions: the involvement of glycoprotein VI in the platelet adhesion. *Blood* 88(6):2081–92.

APPENDIX A

Shear Rate (s^-1)	R1 D1	R2 D1	R3 D1	R1 D2	R2 D2	R3 D2	R1 D3	R2 D3	R3 D3	R1 D4	R2 D4	R3 D4	R1 D5	R2 D5	R3 D5	R1 D6	R2 D6	R3 D6
10	1	-	-	3	-	-	3	-	-	4	-	-	0	-	-	1	-	-
91.36	4	1	1	7	2	20	2	6	1	0	0	3	3	0	3	0	2	0
199.72	2	5	2	15	7	19	1	2	15	2	0	0	2	1	2	0	2	1
286.08	0	6	0	5	12	20	2	9	1	1	0	1	0	1	0	0	0	0
381.44	4	7	0	7	5	9	0	2	4	1	1	0	0	1	4	0	2	2
482.8	11	0	1	2	19	0	1	5	11	0	0	0	25	0	15	1	1	2
529.16	22	1	8	2	5	0	0	0	9	14	2	7	121	0	354	0	0	6
626.52	12	0	1	6	2	52	1	1	0	1	15	9	4	2	268	0	0	1
722.88	-	27	0	0	0	2	0	0	2	1	4	11	78	3	101	0	0	0
755.24	-	11	1	0	0	2	0	0	0	0	0	0	1	0	36	1	0	0

Table A.1 Raw platelet counts for 20% Hct for 0.5 hours.

Shear Rate (s^-1)	Average	St. Dev.	SEM
10	2	1.549193	0.632456
91.36	3.055556	3.342764	1.364678
199.72	4.333333	4.966555	2.027588
286.08	3.222222	4.698305	1.918075
381.44	2.722222	2.322993	0.948358
482.8	5.222222	4.754725	1.941108
529.16	30.61111	62.65972	25.58072
626.52	20.83333	35.28849	14.40647
722.88	13.47222	23.67709	9.666132
755.24	3.222222	5.027333	2.0524

Table A.2 Average platelet counts for 20% Hct for 0.5 hours with standard deviation and SEM.

$y = 3.827\ln(x) - 11.419$
$R^2 = 0.2607$
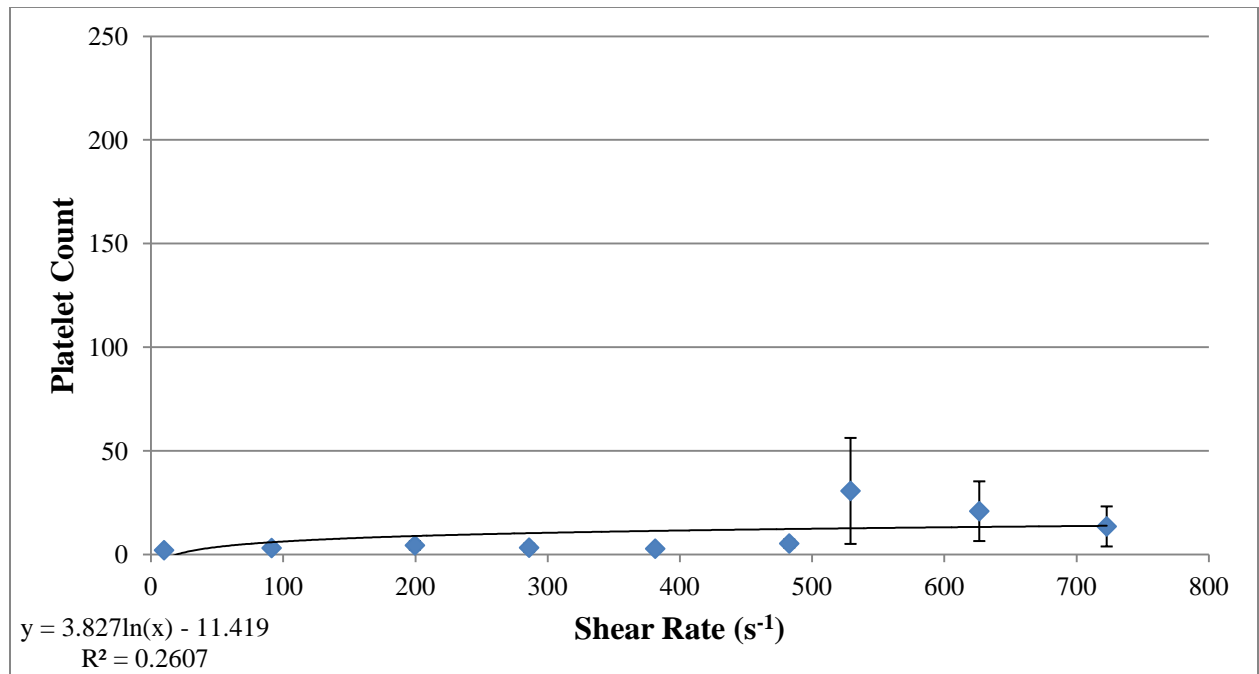
Figure A.1 Platelet count versus shear rate for 20% Hct for 0.5 hours.

Shear Rate (s^-1)	R1 D1	R2 D1	R3 D1	R1 D2	R2 D2	R3 D2	R1 D3	R2 D3	R3 D3	R1 D4	R2 D4	R3 D4	R1 D5	R2 D5	R3 D5	R1 D6	R2 D6	R3 D6
22	9	-	-	5	-	-	0	-	-	0	-	-	2	-	-	5	-	-
38.372	3	0	1	11	13	13	1	2	2	0	0	2	2	5	1	42	5	15
122.74	0	0	7	6	6	5	1	0	1	0	0	0	1	1	2	4	1	4
207.12	0	8	0	52	13	2	3	1	0	1	1	0	1	2	0	5	5	19
305.49	0	5	0	95	3	0	0	1	1	0	0	0	4	0	0	24	11	4
401.86	0	0	0	482	133	2	0	1	0	1	1	1	8	0	0	6	11	11
517.23	0	0	0	335	4	4	1	0	5	0	0	0	0	0	1	29	47	0
611.61	0	0	0	414	3	82	0	2	1	0	0	0	0	1	0	5	20	23
715.98	0	0	1	457	108	2	0	0	0	1	2	0	0	0	0	7	10	24
866.35	0	0	0	463	23	5	0	1	0	0	0	2	0	0	0	85	198	2

Table A.3 Raw platelet counts for 40% Hct for 0.5 hours.

Shear Rate (s^-1)	Average	St. Dev.	SEM
22	3.5	3.507136	1.431782
38.372	6.555556	8.16678	3.334074
122.74	2.166667	2.030326	0.828877
207.12	6.277778	8.556782	3.493292
305.49	8.222222	12.92657	5.277251
401.86	36.5	82.9465	33.86277
517.23	23.66667	45.51337	18.58075
611.61	30.61111	66.7857	27.26515
715.98	34	76.12212	31.07673
866.35	43.27778	70.1064	28.62082

Table A.4 Average platelet counts for 40% Hct for 0.5 hours with standard deviation and SEM.
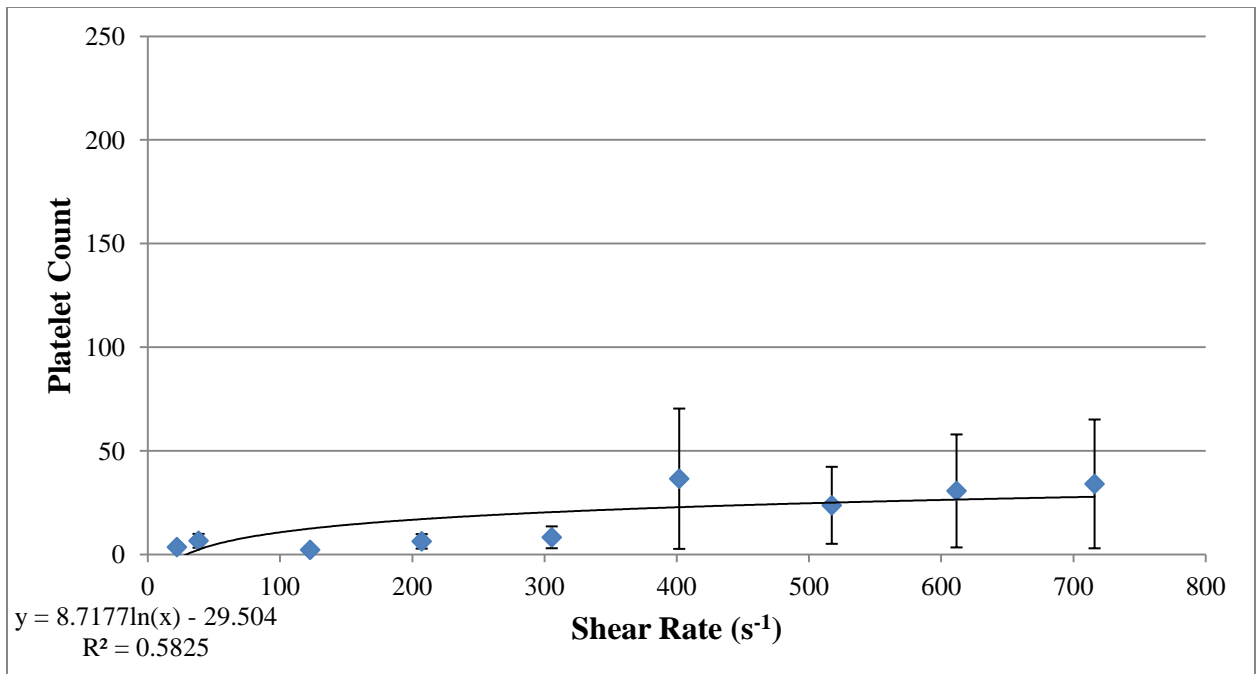
Figure A.2 Platelet count versus shear rate for 40% Hct for 0.5 hours.

Shear Rate (s^-1)	R1 D1	R2 D1	R3 D1	R1 D2	R2 D2	R3 D2	R1 D3	R2 D3	R3 D3	R1 D4	R2 D4	R3 D4	R1 D5	R2 D5	R3 D5	R1 D6	R2 D6	R3 D6
10	5	-	-	7	-	-	6	-	-	4	-	-	2	-	-	2	-	-
91.36	2	18	25	25	18	2	5	4	5	70	84	55	4	3	3	112	28	74
199.72	6	27	48	12	13	6	17	16	13	163	163	174	2	2	1	3	10	31
286.08	1	61	51	5	4	1	4	0	11	202	172	217	2	0	0	64	5	114
381.44	0	149	46	10	3	64	3	8	0	212	252	302	11	1	1	302	3	6
482.8	0	104	9	38	7	74	4	12	0	276	285	302	3	0	1	8	13	53
529.16	0	106	28	5	28	22	2	9	0	258	276	372	0	3	0	266	6	0
626.52	0	5	25	25	6	41	5	4	37	357	299	492	0	1	0	21	333	7
722.88	2	217	24	31	0	36	0	15	11	254	209	435	0	0	0	312	194	1
755.24	0	3	0	21	0	0	0	0	1	288	101	-	2	1	0	64	221	0

Table A.5 Raw platelet counts for 20% Hct for 1 hour.

Shear Rate (s^-1)	Average	St. Dev.	SEM
10	4.333333333	2.065591118	0.843274043
91.36	29.83333333	31.88921796	13.01871872
199.72	39.27777778	62.94456703	25.69701188
286.08	50.77777778	75.51825877	30.83020004
381.44	76.27777778	95.86249798	39.13570092
482.8	66.05555556	109.7296509	44.79694241
529.16	76.72222222	115.2842702	47.06460624
626.52	92.11111111	148.941848	60.80525481
722.88	96.72222222	117.6139479	48.01569317
755.24	49.80555556	80.02849608	32.67149671

Table A.6 Average platelet counts for 20% Hct for 1 hour with standard deviation and SEM.
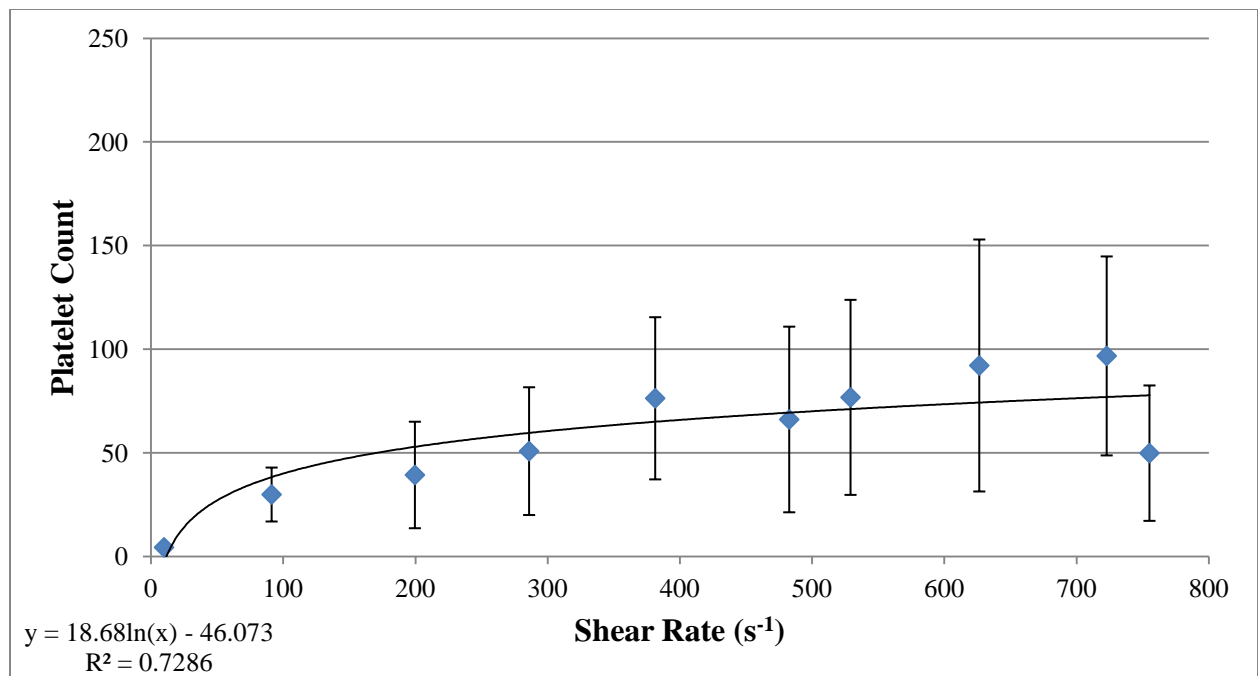
y = 18.68ln(x) - 46.073
R² = 0.7286

Figure A.3 Platelet count versus shear rate for 20% Hct for 1 hour.

Shear Rate (s^-1)	R1 D1	R2 D1	R3 D1	R1 D2	R2 D2	R3 D2	R1 D3	R2 D3	R3 D3	R1 D4	R2 D4	R3 D4	R1 D5	R2 D5	R3 D5	R1 D6	R2 D6	R3 D6
22	1	-	-	2	-	-	0	-	-	1	-	-	2	-	-	2	-	-
38.372	11	6	4	2	5	0	4	2	3	3	2	3	5	0	3	2	0	3
122.74	0	17	14	2	2	3	5	3	2	1	2	3	5	0	0	1	1	2
207.12	1	29	0	0	1	0	2	4	3	1	0	0	4	8	9	3	3	0
305.49	81	0	1	0	5	2	0	2	2	0	0	1	0	43	42	2	0	0
401.86	3	95	88	0	11	0	7	0	2	0	0	0	0	32	61	0	0	0
517.23	3	103	2	0	8	5	0	1	0	1	0	0	11	0	0	0	0	0
611.61	0	335	12	2	1	14	2	0	0	0	0	0	0	14	0	1	0	0
715.98	4	170	17	3	0	5	0	0	0	0	0	0	0	0	0	1	1	0
866.35	0	4	4	0	1	0	0	0	0	0	0	0	1	0	0	1	0	2

Table A.7 Raw platelet counts for 40% Hct for 1 hour.

Shear Rate (s^-1)	Average	St. Dev.	SEM
22	1.333333333	0.816496581	0.333333333
38.372	3.222222222	1.905158689	0.777777778
122.74	3.5	3.417276368	1.395097235
207.12	3.777777778	3.913887903	1.597838046
305.49	10.05555556	13.79116733	5.630220486
401.86	16.61111111	25.18678372	10.2824614
517.23	7.444444444	14.11329817	5.76172985
611.61	21.16666667	46.35742779	18.92534064
715.98	11.16666667	25.74037037	10.5084622
866.35	0.722222222	1.020167016	0.41648144

Table A.8 Average platelet counts for 40% Hct for 1 hour with standard deviation and SEM.
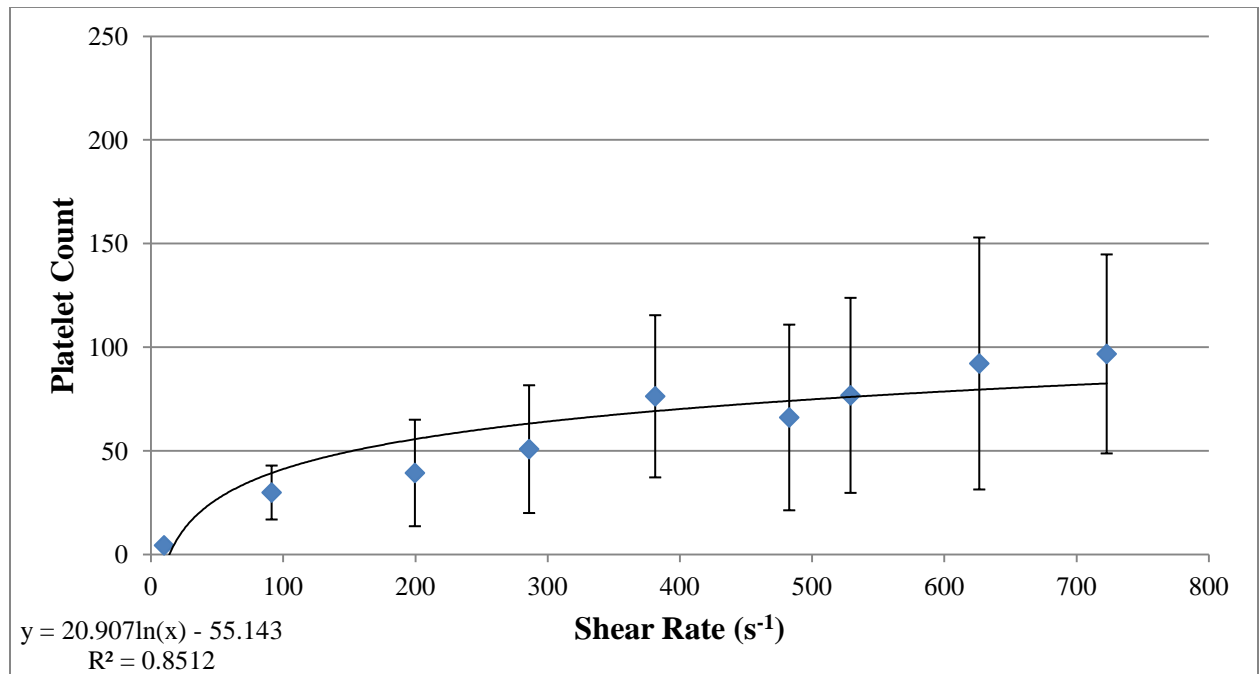
$y = 20.907\ln(x) - 55.143$
$R^2 = 0.8512$

Figure A.4 Platelet count versus shear rate for 40% Hct for 1 hour.

Shear Rate (s^-1)	R1 D1	R2 D1	R3 D1	R1 D2	R2 D2	R3 D2	R1 D3	R2 D3	R3 D3	R1 D4	R2 D4	R3 D4	R1 D5	R2 D5	R3 D5	R1 D6	R2 D6	R3 D6
10	4	-	-	19	-	-	23	-	-	3	-	-	31	-	-	2	-	-
91.36	81	66	56	151	2	54	2	18	13	10	1	17	44	65	26	123	123	73
199.72	0	81	250	63	5	108	1	48	95	43	144	61	103	62	32	199	207	0
286.08	0	16	174	312	308	38	110	0	0	275	219	384	101	6	160	199	126	229
381.44	1	81	237	399	126	283	144	215	2	55	327	240	139	160	186	126	174	274
482.8	6	48	5	316	10	501	48	106	27	32	234	119	62	16	410	283	0	231
529.16	1	141	35	60	94	311	2	91	4	12	38	368	16	72	2	176	30	367
626.52	68	4	68	96	520	206	0	28	0	259	0	590	191	212	199	282	1	286
722.88	17	380	325	341	527	465	34	0	1	7	0	51	236	17	581	35	7	262
755.24	3	0	226	357	482	484	5	341	0	41	0	0	0	36	0	0	1	54

Table A.9 Raw platelet counts for 20% Hct for 2 hours.

Shear Rate (s^-1)	Average	St. Dev.	SEM
10	13.66667	12.32342	5.031015
91.36	51.38889	37.50936	15.31313
199.72	83.44444	33.47348	13.66549
286.08	147.6111	100.4042	40.98983
381.44	176.0556	60.14258	24.5531
482.8	136.3333	90.31427	36.87064
529.16	101.1111	69.28994	28.2875
626.52	167.2222	114.7962	46.86534
722.88	182.5556	169.3846	69.15097
755.24	112.7778	166.1105	67.81433

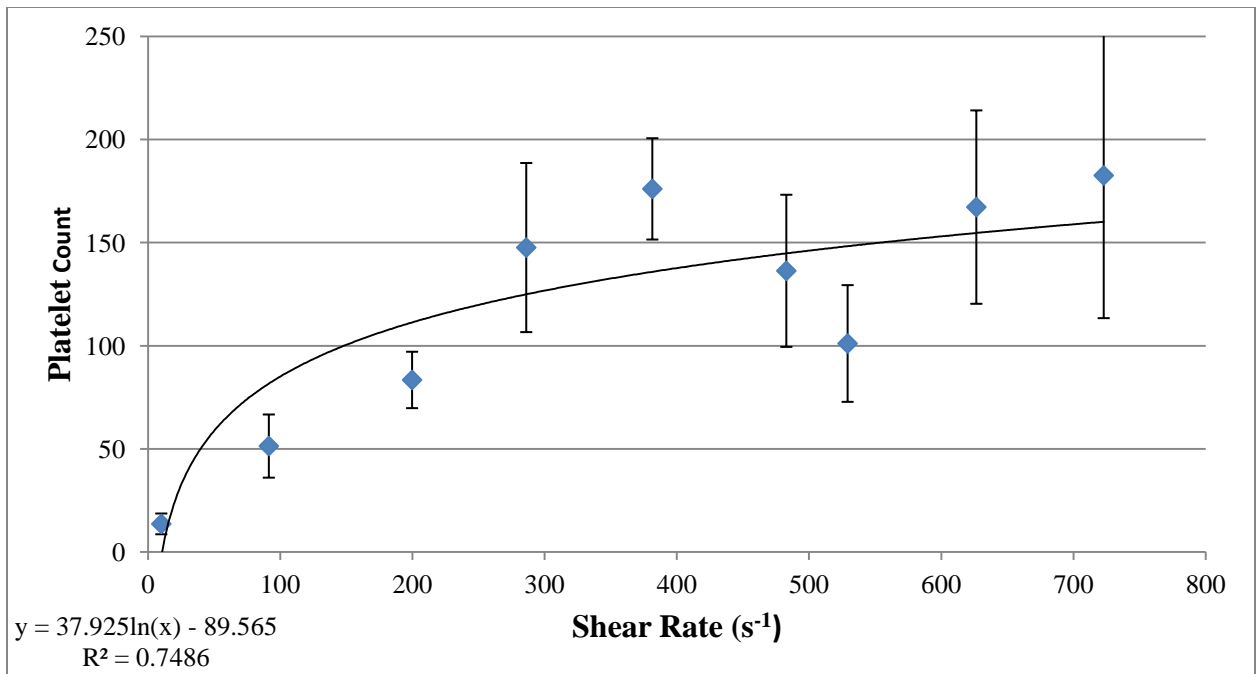**Table A.10 Average platelet counts for 20% Hct for 2 hours with standard deviation and SEM.**

y = 37.925ln(x) - 89.565
R² = 0.7486

Figure A.5 Platelet count versus shear rate for 20% Hct for 2 hours.

Shear Rate (s^-1)	R1 D1	R2 D1	R3 D1	R1 D2	R2 D2	R3 D2	R1 D3	R2 D3	R3 D3	R1 D4	R2 D4	R3 D4	R1 D5	R2 D5	R3 D5	R1 D6	R2 D6	R3 D6
22.00	10	-	-	2	-	-	23	-	-	2	-	-	132	-	-	2	-	-
38.37	9	3	7	4	19	21	38	51	20	73	15	43	216	16	38	100	156	198
122.74	30	4	3	4	1	32	11	47	28	19	103	72	209	426	259	291	330	344
207.12	12	71	29	20	1	41	60	2	55	268	75	200	19	395	386	338	383	337
305.49	1	4	15	2	47	40	2	8	50	137	73	95	124	505	372	356	315	375
401.86	5	0	158	14	12	66	14	0	0	61	44	172	458	349	471	335	469	156
517.23	4	7	150	8	19	1	39	0	10	13	246	62	399	294	429	480	177	473
611.61	3	0	169	4	17	11	16	1	9	29	29	167	574	361	349	592	348	45
715.98	0	0	0	7	0	15	2	11	2	2	150	249	532	502	297	513	148	371
866.35	1	0	0	64	9	0	0	0	11	13	2	246	163	384	563	673	482	624

Table A.11 Raw platelet counts for 40% Hct for 2 hours.

Shear Rate (s^-1)	Average	St. Dev.	SEM
22	28.5	51.36438	20.96942
38.372	57.05556	54.68431	22.32478
122.74	122.9444	146.2116	59.69065
207.12	149.5556	139.5612	56.97561
305.49	140.0556	159.2917	65.03056
401.86	154.6667	174.8057	71.36412
517.23	156.1667	173.2678	70.73627
611.61	151.3333	180.3758	73.6381
715.98	155.6111	193.8209	79.12706
866.35	179.7222	246.1395	100.486

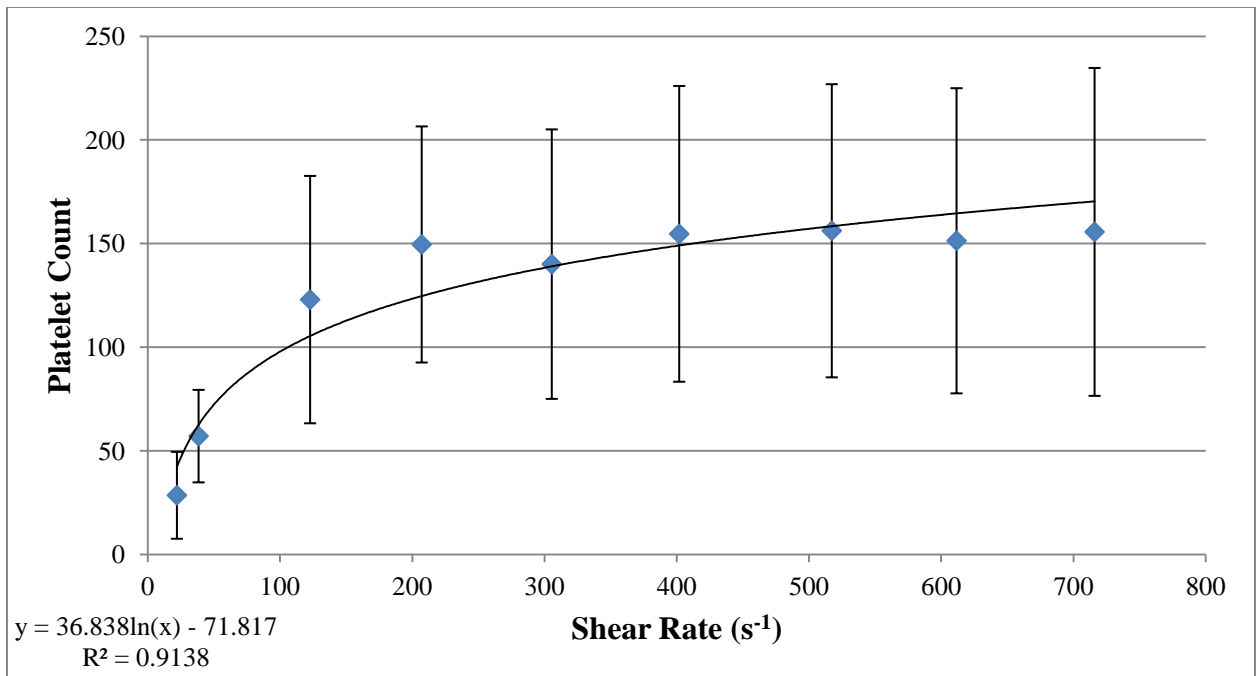**Table A.12 Average platelet counts for 20% Hct for 2 hours with standard deviation and SEM.**

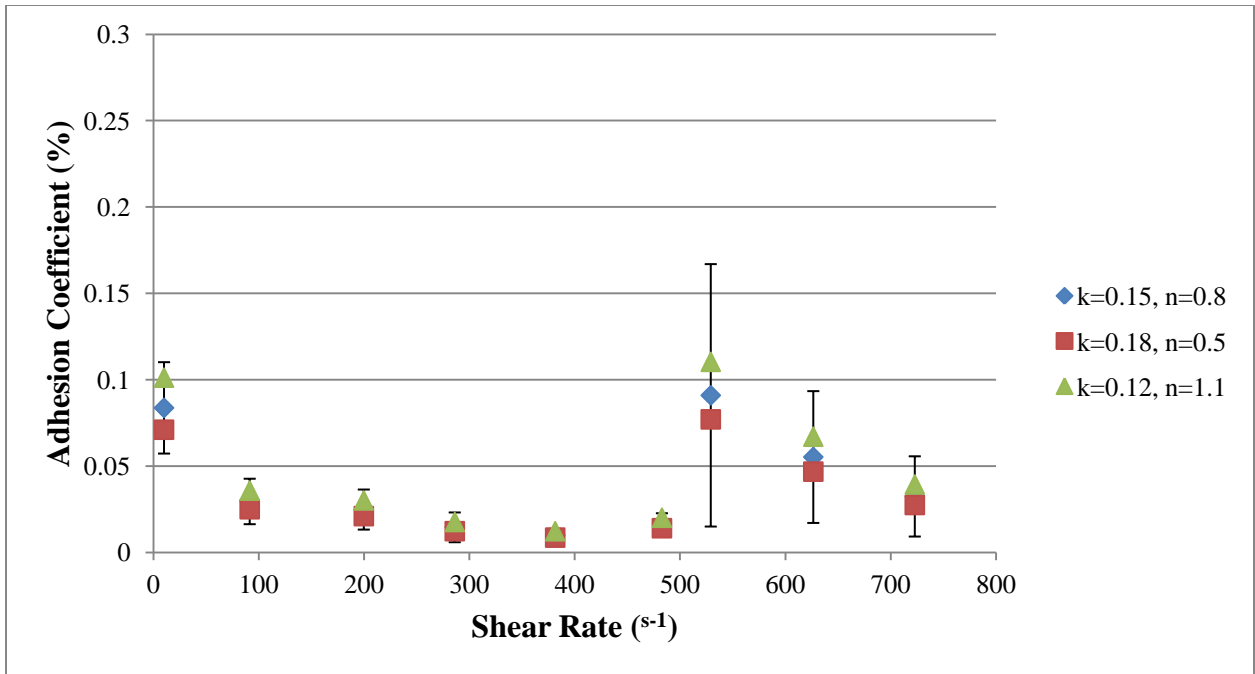**Figure A.6 Platelet count versus shear rate for 40% Hct for 2 hours.**

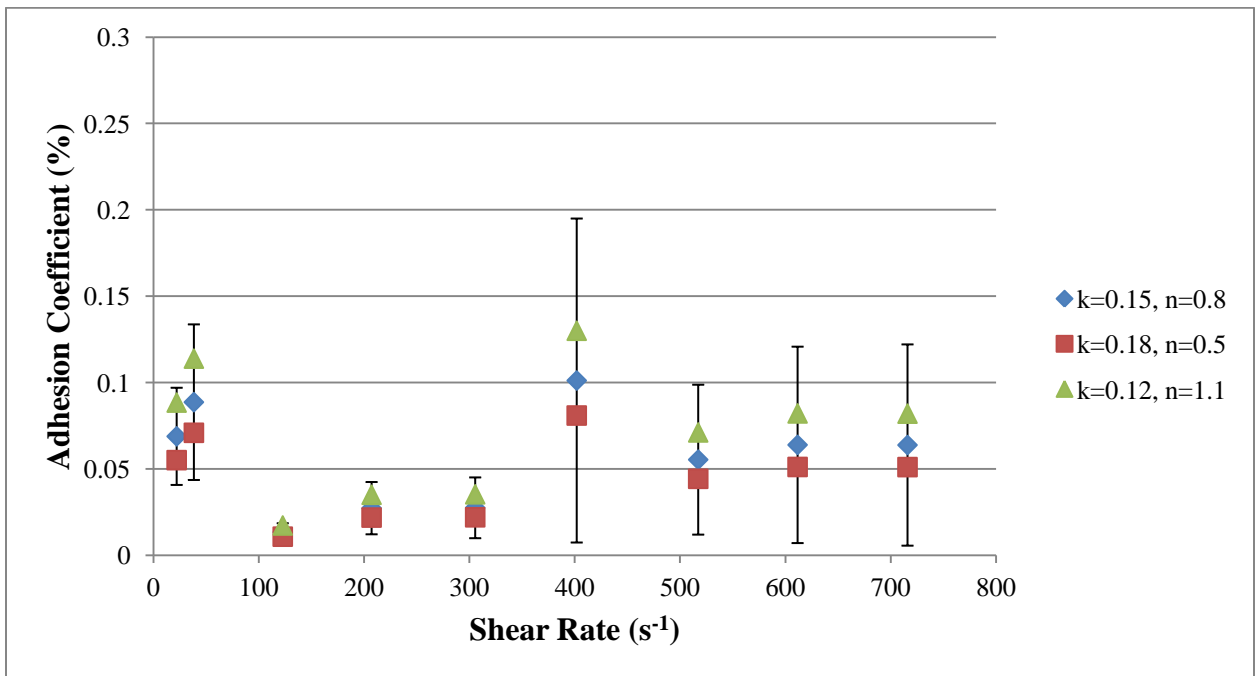**Figure A.7 Adhesion coefficient versus shear rate for 20% Hct, 0.5 hours.**

Figure A.8 Adhesion coefficient versus shear rate for 40% Hct, 0.5 hours.
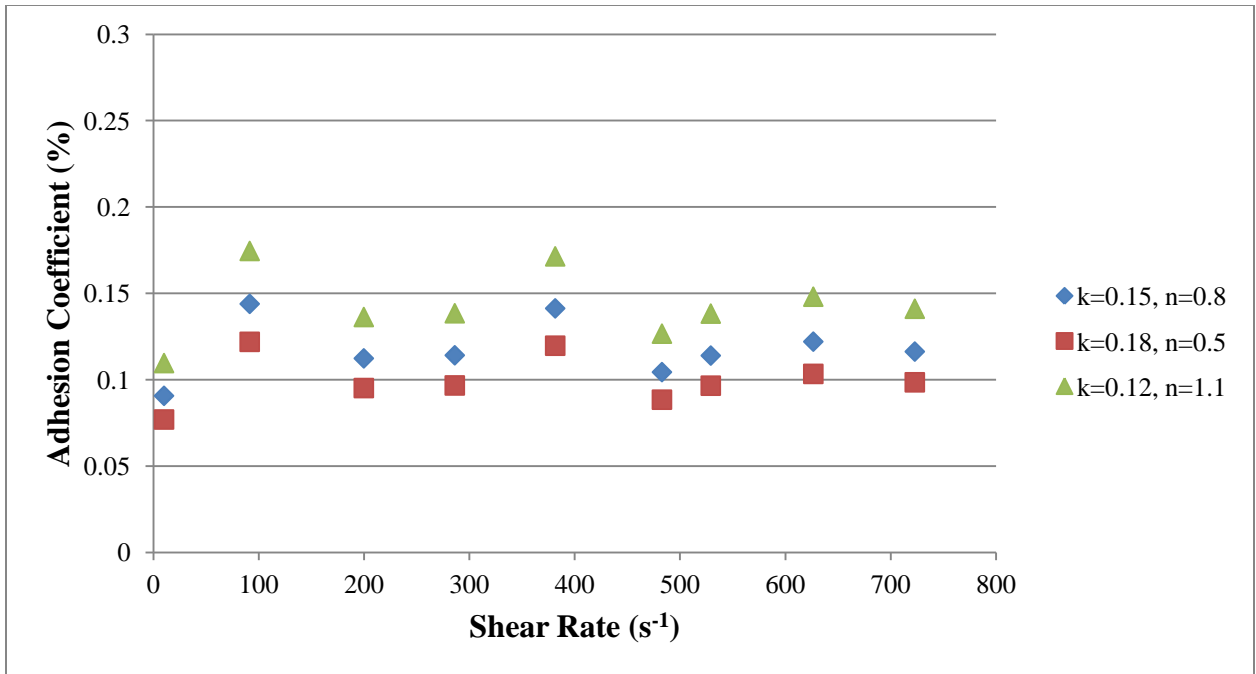
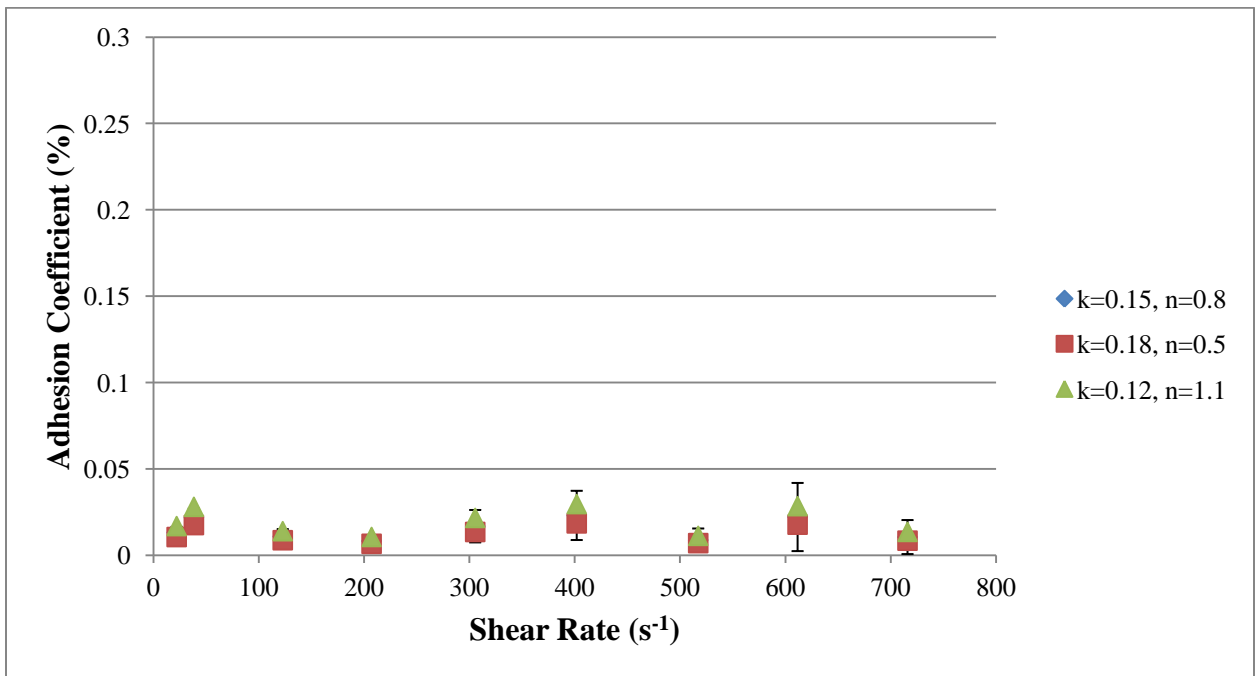**Figure A.9 Adhesion coefficient versus shear rate for 20% Hct, 1 hour.**

Figure A.10 Adhesion coefficient versus shear rate for 40% Hct, 1 hour.

67

Lauren E. Grunenwald
Academic Vita

Local Address	lgrunenwald@gmail.com	Permanent Address
730 N. Atherton Street	412.735.8680	6002 Deer Run Drive
State College, PA 16803		Trafford, PA 15085

Education

M.S. in Bioengineering
The Pennsylvania State University, University Park, PA

B.S. in Bioengineering
The Schreyer Honors College
The Pennsylvania State University, University Park, PA

Research Experience

Graduate Research Assistant (May 2012-Present)
Artificial Heart and Cardiovascular Fluid Dynamics Lab, Penn State University, University Park, PA
- Study platelet adhesion to polyurethane urea, the blood contacting material in the Penn State 50 cc ventricular assist device, under varying flow conditions and physiological parameters using a rotating disk system and confocal microscopy

Honors Undergraduate Research Assistant (September 2009-May 2012)
Artificial Heart and Cardiovascular Fluid Dynamics Lab, Penn State University, University Park, PA
- Constructed mock circulatory loops to model the pediatric cardiovascular system
- Studied the flow fields within the Penn State pediatric ventricular assist device using particle image velocimetry and processed the data to obtain global velocity maps and shear rate plots using MATLAB, Insight 3G, and Tecplot software

Teaching Experience

Graduate Teaching Assistant (January 2013-Present)
Bioengineering Department, Penn State University, University Park, PA
- Assist in teaching 60 undergraduate bioengineering students how to computationally model bioengineering problems using COMSOL Multiphysics, a finite element analysis software, & to analyze data sets using Minitab, a statistical analysis software
- Hold biweekly office hours, create PowerPoint presentations, grade assignments, & proctor lab practicals

Biothermodynamics Teaching Intern (August 2011-December 2011)
Bioengineering Department & The Leonhard Center, Penn State University, University Park, PA
- Led weekly office hours and review sessions focused on fundamental thermodynamics and heat transfer concepts with an emphasis on biomedical applications for 50+ undergraduate bioengineering students
- Developed communication, lesson planning, and teaching skills by attending weekly seminars, created assignments, and lectured about using pressure-volume loops to determine heart function

Clinical Experience

Penn State Milton S. Hershey Summer Clinical Preceptorship Program (June 2012)
- Shadowed physicians in the pediatric primary care clinic, pediatric intermediate care unit, pediatric rheumatology department, pediatric pulmonology department, and family and community medicine clinic
- Checked vital signs and transferred medical information from paper charts to an electronic medical records system

Penn State Milton S. Hershey Medical Center Children's Heart Group (November 2011)
- Shadowed a team of physicians on a 10 day medical mission to the Hospital de Niños in Guayaquil, Ecuador

Conference Presentations

Grunenwald, L.E., Taylor, J.O., Slattery, M.J., Deutsch, S., Siedlecki, C.A., Manning, K.B. The effects of hematocrit and rotation time on platelet adhesion to a polyurethane urea surface. *ASAIO*. Chicago, IL. June 12-15, 2013.

Smith, A.B., Knisely, B.M., Taylor, J.O., **Grunenwald, L.E.**, Deutsch, S., Manning, K.B. *In vitro* shear rate measurements on the surface of a rotating disc for varying non-Newtonian blood analogs. *ASAIO.* Chicago, IL. June 12-15, 2013.

Grants, Awards, & Scholarships

Schreyer Ambassador Travel Grant (2011)
Undergraduate Summer Discovery Grant (2011)
The Evan Pugh Scholar Award (2011)
The President Sparks Award (2010)
The President's Freshman Award (2009)
Henry F. Schoenfeld Scholarship in Engineering (2011-2012)

Schreyer Academic Excellence Scholarship (2008-2012)
Community Women's Club of Level Green Scholarship (2008)
Victor R. Sofelkanik Memorial Scholarship (2008)
Level Green Lions Founders Scholarship (2008)

Extracurricular Activities

Biomedical Engineering Society
- Secretary (2012-2013)
- THON Chair (2012-2013)
- Chemical Engineering Option Mentor (2011-2013)
- Fundraising Co-Chair (2010-2011)
- Member (2008-Present)

Penn State/IFC Panhellenic Dance Marathon (THON)
- Hospitality Committee Canning Chair (2010-2011)
- Member (2009-2011)

Schreyer Honors College Orientation
- Mentor (2009)